Local and substrate-specific S-palmitoylation determines subcellular localization of Gαo

Gonzalo P. Solis[1,*], Jana Valnohova[1], Cecilia Alvarez[2] and Vladimir L. Katanaev[1,3,*]

[1]Translational Research Center in Oncohaematology, Department of Cell Physiology and Metabolism, Faculty of Medicine, University of Geneva, 1211 Geneva, Switzerland;

[2]Centro de Investigaciones en Bioquímica Clínica e Inmunología (CIBICI-CONICET). Departamento de Bioquímica Clínica, Facultad de Ciencias Químicas, Universidad Nacional de Córdoba, Córdoba, Argentina;

[3]School of Biomedicine, Far Eastern Federal University, Vladivostok 690090, Russia;

*Authors for correspondence: gonzalo.solis@unige.ch; vladimir.katanaev@unige.ch.

ABSTRACT

Peripheral membrane proteins (PMPs) associate with cellular membranes through post-translational modifications like S-palmitoylation. The Golgi apparatus is generally viewed as the transitory station where palmitoyl acyltransferases (PATs) modify PMPs, which are then transported to their ultimate destinations such as plasma membrane (PM); little substrate specificity among the many PATs has been determined. Here we describe inherent partitioning of Gαo – α-subunit of heterotrimeric Go-proteins – to PM and Golgi, independent from Golgi-to-PM transport. A minimal code within the Gαo N-terminus governs the compartmentalization and re-coding produces G-protein versions with shifted localization. We established the SpONM (S-palmitoylation at the outer nuclear membrane) assay to probe substrate specificity of PATs in intact cells. With this assay, we showed that PATs localizing to different membrane compartments display remarkable substrate selectivity, which is the basis for specific PMP compartmentalization. Our findings uncover the fundamental mechanism governing protein localization and establish the basis for innovative drug discovery.

INTRODUCTION

G protein-coupled receptors (GPCRs) and their immediate transducers – the heterotrimeric G proteins – have been subjected to intensive scrutiny for decades, primarily due to their pivotal roles in innumerable physiological and pathological processes[1, 2]. Heterotrimeric G proteins are composed of Gα, Gβ and Gγ subunits. The Gα subunit is loaded with either GDP or GTP; the Gβ and Gγ subunits form a constitutive heterodimer that reversibly binds to Gα. GPCRs directly interact with heterotrimeric G proteins on the cytosolic surface of the membrane. Upon activation, GPCRs act as exchange factors to enhance the release of GDP from Gα, leading to the binding of GTP and the activation of the Gα subunit. Subsequently, activated Gα dissociates from the receptor and the Gβγ heterodimer, and the free subunits are competent to interact with downstream targets[3].

G protein activation via GPCRs has long been thought to occur exclusively at the plasma membrane (PM). Most recently, however, considerable experimental evidence has accumulated supporting the notion that GPCRs can activate Gα subunits on the Golgi and other compartments[4]. Analogously, activation of the KDEL receptor (KDELR) by cargo from the endoplasmic reticulum (ER) was shown to trigger signal cascades via Gαs and Gαq/11, with KDELR acting as a non-canonical GPCR at the Golgi[5]. Our own work showed that KDELR also binds and activates monomeric Gαo, which in turn enhances the Golgi-to-PM trafficking via small Rab GTPases[6]. Therefore, the subcellular compartmentalization of Gα subunits appears to be of fundamental relevance for their functions. How Gα subunit compartmentalization is achieved and controlled, however, remains poorly understood.

Gα subunits are grouped into four subfamilies based on sequence and functional similarity: Gαs, Gαi, Gαq/11 and Gα12/13[3]. All Gα subunits bind to membranes via fatty acid modifications at the N-terminus, i.e. N-myristoylation and S-palmitoylation[7]. While the majority of Gα subunits are single-palmitoylated, Gαo and other members of the Gαi subfamily are dual-lipidated. N-myristolation occurs co-translationally and results in the attachment of a 14-carbon saturated fatty acid (myristate) to the N-terminal Gly via a stable amide bond[8]. S-palmitoylation on the other hand occurs post-translationally and results in the attachment of a 16-carbon saturated fatty acid (palmitate) to a Cys residue through a reversible thioester linkage[9]. In vertebrates, N-myristolation is catalyzed by two closely related N-myristoyltransferases (NMT1 and NMT2) whose substrate specificities have been intensively studied in recent years[10]. Intracellular S-palmitoylation is catalyzed by a zinc-finger Asp-His-His-Cys domain-containing (zDHHC) family of palmitoyl acyltransferases (PATs)[11]. There is up to 24 zDHHCs described in mammals; opposite to NMTs, their

substrate specificities are far from being well understood, although substantial advance has been made lately[12].

S-palmitoylation of peripheral membrane proteins (PMPs), including Gα subunits, was shown to occur exclusively at the Golgi, where palmitoylated proteins are subsequently transported to the PM[13]. In recent years, however, cumulative data has emerged indicating that some PMPs might undergo local S-palmitoylation on their target compartments, namely the PM or ER[14, 15]. These opposing views appear difficult to reconcile primarily due to the lack of experimental methods allowing visualization of S-palmitoylation in intact cells.

Here, we defined the critical parameters that govern Gαo N-myristolation, S-palmitoylation and subcellular compartmentalization. By engineering a system that allows the ectopic localization of zDHHCs to the outer nuclear membrane, we showed an intriguing substrate specificity of several zDHHCs towards closely related substrates. Moreover, our data indicate that the steady-state localization of Gαo at the PM and Golgi apparatus is the outcome of local S-palmitoylation events. These findings contrast the traditional views that i) S-palmitoylation of PMPs occurs exclusively at the Golgi and ii) serves to drive subsequent PM-directed delivery of such proteins. The unexpected selectivity among different PATs and their substrates we uncover to drive the intracellular localization of PMPs emerges as an attractive target for drug discovery.

RESULTS

The minimal localization code in the N-terminus of Gαo

For its membrane association, the N-terminus of Gαo is lipid modified by N-myristoylation at Gly2 and S-palmitoylation at Cys3[7]. A recent structural analysis identified the recognition sequence of N-Myristoyltransferases (NMTs) as an N-terminal hexapeptide, excluding Met1[16]. This suggest that a minimal membrane-binding information might reside within the first seven residues of Gαo. Thus far, three crystal structures of heterotrimeric Go have been solved[17-19], showing a prominent α-helix in the Gαo N-terminus that extends toward the Gβγ heterodimer. An overlay of the N-terminal region of these three structures revealed a similar ending of the α-helixes, whereas their beginning falls on different residues at positions between 6 to 10 (Supplementary Fig. 1a-c). A similar overlay of the N-terminal region of seven solved structures of Gαi1 – a close Gαo homologue – showed a much more consistent beginning for the α-helix, which starts at residues 7 or 8 (Supplementary Fig. 1d-f). To study if these regions might have specific roles in Gαo membrane association, we generated the following GFP-fusion constructs (Fig. 1a): one including Gαo N-terminal heptapeptide (Gαo-Nt^{7}-GFP), another with the first 31 residues covering the α-helix (Gαo-Nt^{31}-GFP), and the third containing only the α-helix (Gαo-Nt^{8-31}-GFP). These constructs were expressed in the mouse neuroblastoma Neuro-2a cells (N2a) and their localization at the plasma membrane (PM) and Golgi apparatus were compared with the full-length Gαo-GFP[6]. Surprisingly, Gαo-Nt^{7}-GFP localized predominantly at the Golgi, whereas Gαo-Nt^{31}-GFP displayed a more homogenous PM and Golgi distribution similar to Gαo-GFP (Fig. 1b). Quantification of average fluorescence intensities at these compartments confirmed a much higher Golgi and a lower PM localization of Gαo-Nt^{7}-GFP compared to Gαo-Nt^{31}-GFP and Gαo-GFP (Fig. 1c,d). Then, we performed a crude subcellular fractionation of N2a cells expressing the constructs and showed that Gαo-Nt^{7}-GFP, Gαo-Nt^{31}-GFP and Gαo-GFP were similar in the way they partitioned between the cytosolic and membrane fractions (Fig. 1e,f). As opposed to these constructs showing prominent membrane localizations, Gαo-Nt^{8-31}-GFP was spread over the cytosol and nucleus (Supplementary Fig. 1g), indicating that the N-terminal α-helix alone is not sufficient for membrane association.

In the heterotrimeric G protein complex, the N-terminal α-helix of Gα is one of the regions binding to Gβ[20, 21]. Since Gβ tightly interacts with Gγ, which in turn associates to membranes via its C-terminal prenylation[22], we tested if the poor PM localization of Gαo-Nt^{7}-GFP relates to a lack of Gβγ interaction. For this aim, we co-expressed the Gαo constructs together with mRFP-Gβ1 and mRFP-Gγ3 in N2a cells, and immunoprecipitated the GFP-fusions. Full-length Gαo-GFP strongly pulled down Gβ1 and Gγ3, whereas Gαo-Nt^{7}-GFP and Gαo-Nt^{31}-

GFP showed a very faint co-precipitation of Gβγ with no apparent difference between them (Supplementary Fig. 1h). Thus, the preferential localization of Gαo-Nt^{7}-GFP to the Golgi, as opposed to the dual localization of Gαo-Nt^{31}-GFP to Golgi and PM, is independent from Gβγ.

Together, these results indicate that Nt^{7} is sufficient for Gαo overall membrane binding, but it seems to drive the Golgi rather than the PM localization.

Key residues in Gαo-Nt^{7}

We next aimed to decode the intracellular localization of Gαo-Nt^{7} by a systematical point mutation analysis of its key residues. Amino acid substitutions were designed using the GPS-Lipid prediction tool[23]. For instance, we introduced the Gly-to-Leu mutation at position 2 of Gαo-Nt^{7}-GFP as GPS-Lipid predicted very high likelihood for S-palmitoylation at Cys3 in the mutant (not shown). However, the Gly2 mutation led to a complete loss of membrane association as Gαo-G2L-Nt^{7}-GFP evenly spread over the cytosol and nucleus in N2a cells (Fig. 1g). This result reinforces the notion that N-myristoylation is a prerequisite for S-palmitoylation in Gαo^{7}. Consequently, Gαo-G2L-Nt^{7}-GFP appeared almost exclusively at the cytosolic fraction (Fig. 1h,i). We then introduced the Cys-to-Asn mutation at position 3 as GPS-Lipid predicted a high score for N-myristoylation at Gly2 in the mutant (not shown). The resulting Gαo-C3N-Nt^{7}-GFP was predominantly excluded from the nucleus and showed an ER-like distribution with certain accumulation at the Golgi, which might be accounted for by the high membrane density of the cisternae stack (Fig. 1g). Nevertheless, Gαo-C3N-Nt^{7}-GFP appeared mostly at the cytosolic fraction (Fig. 1h,i), confirming that N-myristoylation confers only weak membrane binding properties[8]. Importantly, the localization of Gαo-Nt^{7} mutants impaired in N-myristoylation and S-palmitoylation was emulated by the treatment with the specific inhibitors DDD85646[24] and 2-bromopalmitate (2-BrPal)[25], respectively (Fig. 1j).

The most recent substrate recognition motif for NMTs was described as M^{1}G[^DEFRWY]X[^DEKR][ACGST][KR]^{7}, with ^ denoting exclusion of residues, and X – any amino acid[16] The authors did not exclude the possibility that peptides lacking a positive charge at position 7 might also be accepted by NMTs. Thus, N-myristoylation of Gαo – and all human N-myristoylated Gα subunits – is not in conflict with the lack of a Lys/Arg residue at this position (Fig. 1a). At position 6, a Ser residue is found in Gαo and all its homologues, and Ser is by far the most frequent residue at this position among NMT substrates[16]. Thus, we first introduced point mutations at Ser6 in Gαo-Nt^{7} based on the substrate recognition motif described by Castrec *et al.* and on a previous study indicating that Arg, Asn, Phe, and Val can occupy this position as well[26]. Substitution of Ser6 by Ala, Cys, Gly, or Thr displayed efficient membrane binding in N2a cells (Fig. 1k). Interestingly, the S6C mutant showed a much higher PM localization compared to Gαo-Nt^{7}-GFP (Fig. 1k,l), suggesting that Cys3 and

Cys6 both undergo S-palmitoylation and that PM targeting might be enhanced by the dual S-palmitoylation. N-myristoylation of these mutants was indirectly verified with the inhibitor DDD85646 (Fig. 1k). Conversely, we observed a largely cytosolic and nuclear localization for the constructs in which the Ser6 was substituted by Arg, Asn, Phe and Val (Supplementary Fig. 1i), suggesting that these residues in position 6 make the N-terminal peptide of Gαo a poor substrate for MNTs.

Cysteine position

Intrigued by the S6C mutant, we questioned if the position of the Cys residue within Gαo-Nt^7 might play any role in its subcellular localization. Thus, we moved the Cys3 to positions 4 (MGNC-Nt^7) and 5 (MGNTC-Nt^7), and expressed the GFP constructs in N2a cells. An Asp residue was placed at position 3 following the GPS-Lipid prediction tool (not sown). Unexpectedly, MGNC-Nt^7-GFP displayed a completely different localization than its parental Gαo-Nt^7 (Figs. 1b, 2a). It exhibited PM localization that was not only higher than that of Gαo-Nt^7-GFP, but also of the full-length Gαo-GFP (Figs. 1b, 2b). Moreover, the perinuclear structures labelled by MGNC-Nt^7-GFP showed a much lower co-localization with the Golgi marker GM130 compared to Gαo-Nt^7-GFP (Pearson's correlation; Figs. 1b, 2a,c). Instead, the perinuclear structures containing MGNC-Nt^7-GFP co-localized better with Lactadherin-C2 (mRFP-Lact-C2; Supplementary Fig. 1j,k), a biosensor for phosphatidylserine[27]. These results imply that MGNC-Nt^7-GFP preferentially associates with the PM-derived endocytic rather than the Golgi-derived secretory pathway. The distinct localization of MGNC-Nt^7-GFP was not the result of a major change in the overall membrane binding, as its presence in the membrane fraction was not significantly different from that of Gαo-Nt^7-GFP (Fig. 1h,i). S-Palmitoylation of Cys4 in MGNC-Nt^7-GFP was confirmed by the incubation with the inhibitor 2-BrPal (Fig. 2d). On the other hand, the Cys5 construct MGNTC-Nt^7-GFP localized at the Golgi and cytosol (Fig. 2a,c) but appeared mostly in the cytosolic fraction upon cell fractionation (Fig. 1h,i). Thus, it seems that the Cys5 is not a good substrate for palmitoyl acyltransferases (PATs), as MGNTC-Nt^7-GFP closely resembles the C3N mutant (Fig. 1g-i).

Most intriguingly, the subcellular localization of MGNC-Nt^7 in N2a cells was fully recapitulated in the full-length Gαo when the same mutation was introduced. Specifically, MGNC-Gαo-GFP showed a higher PM targeting (Figs. 1b, 2e,f) and a much lower co-localization with the Golgi marker GM130 (Figs. 1b, 2e,g) than Gαo-GFP.

Altogether, these data uncover a remarkable characteristic of the N-terminal localization code of Gαo: minor changes in its amino acid sequence can drastically modify the subcellular localization of the protein. Due to its homology with all dual lipidated Gα subunits, and to

other similarly modified PMPs, we reasoned that this principle might have a much broader relevance in biology.

The evolution of Gα-Nt^7

Next, we wanted to determine how much diversity is present in Nt^7 among eukaryotic Gα subunits. We searched for Gα sequences containing an N-terminal heptapeptide with the signature M^{1}GXXX[ACGST]X^7, with at least one Cys at positions 3-5 or 7. Of note, we did not find any Gα subunit orthologue in the clades Ancyromonadida, Apusozoa, Breviatea, Cryptophyceae, CRuMs, Glaucocystophyceae, Malawimonadidae, and Rhodophyta (red algae). We found, however, Gα subunits in abundance in Amoebozoa, Discoba, Haptista, Metamonada, Opisthokonta, Sar, and Viridiplantae. Overall, we identified more than 800 sequences containing the desired Nt^7 signature (Supplementary Table 1), and uncovered some interesting features. For instance, no Gα subunits was found with a Cys occupying position 7. On the other hand, we observed Cys throughout positions 3-5, with Cys3 as the most common case with just over half of the sequences. Cys4 follows as the second most frequent with one third of all cases, whereas only ~6% of Gα subunits contain a Cys5. The vast majority of Gα subunits containing a Cys5 are from plants (~65%) and Amoebozoa (~25%). Curiously, Cys5 is not present in Fungi and is almost completely absent in Metazoa, with the genus *Caenorhabditis* as the sole identified exception (e.g. *C. elegans*; Supplementary Table 1). Less than 10% of all sequences present two Cys residues occupying positions 3-5, and they almost exclusively belong to fungal Gα subunits (Supplementary Table 1). A double Cys at positions 3 and 4 is by far the most frequent combination among them. No Gα sequence was found with a Cys occupying all three positions.

We asked whether consensus sequences might emerge from the Gα subunits among each category. As available databases are biased towards certain clades, we first selected unique hexapeptides with the signature M^{1}GXXX[ACGST]^6. When an identical combination within positions 3-5 was found, we selected the sequence with the most frequent residue at position 7 for this analysis. Thus, we identified 88 unique combinations for Cys3, 75 for Cys4, and 13 for Cys5 (Supplementary Table 2). As seen in the corresponding Logo representations, there is no obvious Gα-Nt^7 consensus for the Cys3 and Cys4 categories (Fig. 2h,i), whereas the sequence MGSLCSR emerges for Cys5 (Fig. 2j). Plotting the amino acids by their polarity groups showed a common characteristic among categories: positively and even more so negatively charged amino acids are strongly underrepresented at positions 3-5 compared to a random distribution, or even completely absent as in the Cys5 category (Supplementary Fig. 2a-d). One can speculate that charged amino acids might interfere with at least one of

the lipid modifications of Gα-Nt^7. The most recent recognition motif for NMTs (see above) denotes that positive and negative residues are not favored at certain positions[16]. Accordingly, N-myristoylation of Gαo-Nt^7-GFP appeared strongly impaired in N2a cells when different combinations of Arg, Asp, Glu, or Lys were introduced at positions 4 and 5 (Supplementary Fig. 2e). A Gαo-Nt^7-GFP mutant with a His occupying position 5 showed a near normal membrane association regardless of the presence of a positive or negative residue at position 4 (Supplementary Fig. 2f). Thus, N-myristoylation of Gα-Nt^7 of the Cys3 category appears optimal when Arg, Asp, Glu, or Lys residues are excluded from position 5, in total agreement with the substrate recognition motif described by Castrec *et al*.

As a consensus emerged for the Cys5 category (Fig. 2j), we expressed a GFP-fusion of this sequence in N2a cells. Somehow predictably, MGSLCSR-Nt^7-GFP showed a much better membrane binging than our designed MGNTC-Nt^7-GFP, and localized predominantly at the Golgi (Fig. 2a,k). When MGSLCSR was introduced into the full-length Gαo, however, the membrane association of this mutant was not very efficient (Fig. 2l), probably related to the fact that Gα subunits of the Cys5 category are virtually absent in Metazoa (Supplementary Table 1).

Then, we expressed our constructs Gαo-Nt^7-GFP, MGNTC-Nt^7-GFP and the consensus MGSLCSR-Nt^7-GFP in the *Drosophila* Schneider-2 cell line. Remarkably, all constructs retained the same localization patterns as seen in N2a cells: Gαo-Nt^7 and MGSLCSR-Nt^7 targeted mainly Golgi stacks labelled by GalT-mRFP, while MGNTC-Nt^7 associated largely with the PM (Fig. 2m). Similar localizations were also seen in HeLa cells (Supplementary Fig. 2g). These data point to highly conserved rules for N-myristoylation and S-palmitoylation as well as for substrate compartmentalization.

Direct targeting of Nt^7 variants to Golgi or PM

Our next goal was to understand the molecular mechanism behind the contrasting subcellular localization of two rather similar sequences: Gαo-Nt^7 and MGNC-Nt^7. N-myristoylation generally occurs during protein synthesis and confers a weak membrane binding to the modified protein[25]. N-myristoylation is essential for the subsequent S-palmitoylation to occur[7]. Our own data showed that myristoylated, but not palmitoylated Gαo-Nt^7 and MGNC-Nt^7 are indistinguishable in their localization and only prevented from free cytosolic and nuclear diffusion (Figs. 1j, 2d). Therefore, we speculated that S-palmitoylation is key for subcellular compartmentalization, by itself or in combination with the myristoyl group and/or neighboring amino acids. It has been shown that S-palmitoylation of PMPs – including Gα subunits – occurs exclusively at the Golgi apparatus, the event followed by the transport of PMPs to the PM via the secretory pathway[13]. Thus, one plausible explanation for

the distinct steady-state localizations of Gαo-Nt^7 and MGNC-Nt^7 might involve a differential Golgi-to-PM transport of the constructs.

To test this idea, our first approach was to visualize how these constructs are trafficked in the cell. We adapted to our constructs the reverse dimerization (RD) assay, originally designed for the synchronized trafficking of secretory and integral membrane proteins[28]. This method is based on the aggregation of the F36M mutant of the protein FKBP12 (FM) that allows protein tracking upon chemical dissociation. Thus, we intercalated four FM copies (FM^4) between Nt^7 and GFP, and expressed the constructs in HeLa cells for better visualization. The distinct localization of Gαo-Nt^7 and MGNC-Nt^7 – still observed in HeLa cells (Supplementary Fig. 2g) – was lost by the FM^4 insertion, and cytosolic aggregates of different sizes were visualized instead (Fig. 3a). After chemical dissociation by the D/D solubilizer, most of the aggregates vanished and the constructs showed their characteristic localizations (Fig. 3a).

Then, live imaging was performed in HeLa cells co-expressing each of the Nt^7-FM^4-GFP constructs together with MannII-mRFP, a broader Golgi marker. As expected, Gαo-Nt^7-FM^4-GFP showed a rapid accumulation at the Golgi once the D/D solubilizer was added (Fig. 3b,c and Supplementary Video 1). On the other hand, MGNC-Nt^7-FM^4-GFP presented a rather slow and miniscule accumulation at the Golgi, whereas its PM targeting was much faster (Fig. 3b,c and Supplementary Video 2). This result does not support a Golgi-to-PM flow of MGNC-Nt^7-FM^4-GFP, as PM targeting was not preceded by its Golgi accumulation. To further prove that PM localization of MGNC-Nt^7-FM^4-GFP is indeed independent from transport through the Golgi, we performed the RD assay under the 20°C temperature block that forces cargo to accumulate in the Golgi[29]. As control, we used the GFP-FM^4-hGH construct that aggregates in the ER lumen and is secreted via the Golgi-mediated transport after chemical dissociation[30]. Incubation with D/D solubilizer for 45 min induced an almost complete secretion of GFP-FM^4-hGH at 37°C, while at 20°C the construct strongly accumulated in the Golgi (Fig. 3d). Conversely, HeLa cells expressing MGNC-Nt^7-FM^4-GFP showed a comparable PM localization of the construct at both temperatures (Fig. 3d). Quantification of MGNC-Nt^7-FM^4-GFP mean fluorescence intensity in the MannII-mRFP region revealed no significant difference in its Golgi content at 37°C and 20°C (Fig. 3e), supporting the notion that PM targeting of MGNC-Nt^7 does not occur via transport through Golgi.

Altogether, these results imply that the characteristic steady-state localizations of Gαo-Nt^7 and MGNC-Nt^7 are not related to the Golgi-to-PM trafficking. Instead, each of the constructs goes directly to its primary destination: Golgi or PM.

Lipid binding of Nt^7 variants does not explain the preferential localization

Thus far, our data indicate that S-palmitoylation might contribute to the compartmentalization of Gαo-Nt^7 and MGNC-Nt^7, and that intracellular trafficking is not a major player in their distinctive localizations. We then envisioned two further scenarios that could explain the differential Nt^7 compartmentalization: (i) PATs have no specificity for substrate recognition, and the substrates concentrate at different compartments due to specific interactions, and (ii) PATs discriminate substrates, which in turn accumulate at the compartment where S-palmitoylation takes place. The first scenario involves a certain degree of promiscuity among PATs[12], and implies that lipidations and a few surrounding amino acids confer specific binding properties e.g. to lipids, which are known to differentially accumulate all over the endomembrane system[31]. Additionally, fatty acids other than palmitate can also be attached to the available Cys and might confer different binding specificities to the S-acylated protein[32]. The second scenario requires that PATs discriminate between analogous substrates as small as Nt^7 and that a given substrate accumulates at the compartment where its specific PAT is localized.

To test the first scenario, we used commercially available membrane strips spotted with fifteen different lipids found in cellular membranes and performed a protein-lipid overlay assay[33]. As control, we employed a GFP-fusion of the pleckstrin homology (PH) domain of FAPP1 (FAPP1-PH-GFP), that specifically binds to phosphatidylinositol 4-phosphate (PI4P)[34]. N2a cells were transfected with Gαo-Nt^7-GFP, MGNC-Nt^7-GFP or FAPP1-PH-GFP, and then membrane strips were incubated with cleared cell extracts. As expected, FAPP1-PH-GFP showed a strong binding to the spot containing PI4P (Supplementary Fig. 3a). On the other hand, no apparent difference was found for Gαo-Nt^7-GFP and MGNC-Nt^7-GFP that mainly bound to phosphatidylserine, cardiolipin, and phosphoinositides, particularly to PI4,5P2 (Supplementary Fig. 3a). A similar lipid-binding pattern was also observed by the larger construct Gαo-Nt^{31}-GFP (Supplementary Fig. 3a). Thus, the compartmentalization of Gαo-Nt^7 and MGNC-Nt^7 is unlikely to emerge from different lipid-binding affinities, arguing against the first scenario.

A novel tool for visualization of local S-palmitoylation in intact cells

Next, we studied the second scenario, which implies that local S-palmitoylation drives substrate compartmentalization. In mammals, intracellular S-palmitoylation is mediated by 23-24 zDHHC proteins with PAT activity[11]. Most of the zDHHCs have four transmembrane domains (TMDs), whereas only two and three members present five and six TMDs, respectively[12]. The majority of zDHHCs localize at the Golgi and the remaining are distributed among the ER, PM and endosomes[35, 36]. In order to confirm their subcellular localization, we

expressed a collection of twenty-three HA-tagged mouse zDHHCs in N2a cells[37]. As expected, immunostainings revealed that a large number of zDHHCs localized predominantly at the Golgi: zDHHC3, 7, 9, 12, 13, 15-17, 21, 23, and 25 (Supplementary Fig. 3b). Six showed a clear PM localization but were also found on endosomes: zDHHC2, 5, 11, 14, 18, and to a lesser extent zDHHC8. The rest of the PATs mostly showed an ER localization, while zDHHC4 associated almost exclusively with the nuclear envelope (Supplementary Fig. 3b), a pattern not described in previous studies[35, 36].

Beside from a unique antibody that specifically recognizes palmitoylated PSD-95[38], experimental approaches to study zDHHC-substrate pair relations are based exclusively on disruptive biochemical and proteomic techniques[39, 40]. To determine if Gαo-Nt[7] and MGNC-Nt[7] are differently lipidated at the PM *vs*. Golgi, we aimed at developing a method to visualize local S-palmitoylation in intact cells. Inspired by the nuclear envelope localization of zDHHC4, we engineered zDHHCs that ectopically target the outer nuclear membrane (ONM) to detect mislocalized substrates. We took advantage of some components of the well-studied LINC (linker of nucleoskeleton and cytoskeleton) complexes. LINC complexes are built by proteins of the KASH (Klarsicht, ANC-1, and Syne Homology) family that are embedded in the ONM and interact within the perinuclear space with proteins of the SUN (Sad1 and UNC-84) family, which in turn are inserted in the inner nuclear membrane[41]. As the C-terminus of all zDHHCs except zDHHC24 faces the cytosol, we hypothesized that addition of a C-terminal KASH-domain might induce their targeting to the ONM (Fig. 4a). To test this hypothesis, we first generated a zDHHC5 construct carrying an N-terminal mRFP for visualization and the KASH-domain of syne-1/nesprin-1 at its C-terminus (mRFP-zDHHC5-KASH; Fig. 4a). In HeLa cells, the KASH-domain alone (mRFP-KASH) is efficiently targeted to the ONM (Fig. 4b), and mRFP-zDHHC5 localized at the PM and endosomes as expected (Fig. 4b and Supplementary Fig. 3b). The addition of the KASH domain strongly impaired PM localization of zDHHC5, but a robust ONM targeting was only achieved by the co-expression of the KASH-interacting protein SUN2 (Fig. 4b).

Next, we analyzed if known zDHHC-substrate pair relations can be recapitulated in HeLa cells and chose the PMPs SNAP23, caveolin-1 and flotillin-2. The core of SNAP23 contains 6 Cys residues that are plamitoylated by zDHHC13 and 17[42]. zDHHC7 appears as the main PAT for caveolin-1, which is plamitoylated in 3 Cys residues at its C-terminus[43]. Flotillin-2 is myristoylated at Gly2 and palmitoylated at Cys4, 19 and 20 by zDHHC5[44]. Remarkably, the GFP-fusions of SNAP23 (Supplementary Fig. 4a), caveolin-1 (Supplementary Fig. 4b) and flotillin-2 (Supplementary Fig. 4c) were efficiently recruited to the ONM by the corresponding zDHHC-KASH constructs. Together, we successfully developed a system in intact cells for the visualization of local S-palmitoylation at the ONM (henceforth SpONM).

Compartment-specific S-palmitoylation of Nt^7

Once the SpONM system was established, we first tested if PM-associated zDHHCs showed differential substrate specificities for Gαo-Nt^7 and MGNC-Nt^7. In addition to zDHHC5, the C-terminal KASH-domain effectively targeted zDHHC2, 8, 11, 14 and 18 to the ONM (Fig. 4c,d and Supplementary Fig. 4d). Remarkably, Gαo-Nt^7-GFP and MGNC-Nt^7-GFP were efficiently recruited to the ONM by the co-expression of mRFP-zDHHC11-KASH but not by the control mRFP-KASH (Fig. 4c,d). To quantify these effects, we measured the mean GFP-fluorescence intensity at the ONM and nearby cytosol, and used their ratio to determine the relative ONM content of the Nt^7 constructs. Quantification revealed a similar ~2.5-fold accumulation of Gαo-Nt^7-GFP and MGNC-Nt^7-GFP at the ONM by the co-expression of mRFP-zDHHC11-KASH (Fig. 4e), suggesting that zDHHC11 equally accepts both Nt^7 constructs as substrate and identifying this enzyme as the major PM-localized PAT for Gαo. On the other hand, the KASH-fusions of zDHHC2, 5, 8, 14 and 18 showed no effect on the localization of Gαo-Nt^7-GFP and MGNC-Nt^7-GFP (Supplementary Fig. 4d). Thus, it appears that the predominant PM localization of MGNC-Nt^7 cannot be explained by major differences in substrate specificity of PM-associated zDHHCs.

Next, we applied the SpONM system to Gαo-Nt^7 and MGNC-Nt^7 using the eleven Golgi-associated zDHHCs, as all were efficiently targeted to the ONM by the C-terminal KASH-domain (Fig. 4f,g and Supplementary Fig. 5a,b). Notably, the mRFP-zDHHC-KASH constructs for zDHHC3 and 7 caused a strong ONM accumulation of Gαo-Nt^7-GFP (Fig. 4f,g). No other zDHHCs showed any activity toward Gαo-Nt^7-GFP (Supplementary Fig. 5a), suggesting a high degree of specificity in substrate recognition among Golgi-associated PATs and identifying zDHHC3 and 7 as the major Golgi-localized PATs for Gαo. MGNC-Nt^7-GFP was, however, only slightly recruited to the ONM by the KASH-fusions of zDHHC3 and 7 (Fig. 4f,g), and completely absent from the ONM by the co-expression of the remaining Golgi zDHHC-KASH constructs (Supplementary Fig. 5b). Quantification showed that Gαo-Nt^7-GFP accumulates at the ONM roughly 2.0 and 2.5 folds by the co-expression of zDHHC3 and zDHHC7, respectively (Fig. 4h,i). Conversely, MGNC-Nt^7-GFP presented a significantly lower ONM recruitment of ~1.5 folds by both zDHHC3 and 7 (Fig. 4h,i).

To confirm that the PAT activity was responsible for the mislocalization of substrates in the SpONM system, we generated zDHHC-inactive constructs by a Cys-to-Ser mutation in the catalytic DHHC domain[37]. As anticipated, the ability of the KASH-fusions of zDHHC3, 7 and 11 to induce ONM accumulation of Gαo-Nt^7 and MGNC-Nt^7 was completely abolished when DHHS-mutants were co-expressed (Fig. 5a). Together, our data suggest that the distinct steady-state localizations of Gαo-Nt^7 and MGNC-Nt^7 are due to the differential substrate

specificities of PM- and Golgi-localized zDHHCs. This notion implies that the localization of Nt^7 constructs might be shifted toward the PM or Golgi by manipulating the expression level of specific zDHHCs. To test this hypothesis, we co-transfected N2a cells with Gαo-Nt^7-GFP and HA-zDHHC11, and determined its relative PM content and co-localization with the MannII-BFP Golgi marker. We also co-expressed MGNC-Nt^7-GFP together with HA-zDHHC3 or HA-zDHHC7. Remarkably, the PM localization of Gαo-Nt^7 strongly increased by the overexpression of zDHHC11, whereas its co-localization with MannII-BFP showed a significant decrease (Fig. 5b,e,f). On the other hand, MGNC-Nt^7 presented a higher co-localization with the Golgi marker but a significant decrease in PM content by the co-expression of zDHHC3 or zDHHC7 (Fig. 5c-f). The effects of the different zDHHCs on the steady-state localization of Gαo-Nt^7 and MGNC-Nt^7 were not evident upon co-expression of the corresponding DHHS-mutants (Fig. 5b-f), since both Nt^7 constructs showed similar localization patterns as described above (Figs. 1b, 2a-c). Collectively, these data confirm the notion that local S-palmitoylation plays a major role in the compartmentalization of Gαo-Nt^7 and MGNC-Nt^7. As the KASH-fusion of zDHHC11 was able to target both Gαo-Nt^7 and MGNC-Nt^7 to the ONM (Fig. 4c-e), we asked whether it might not discriminate among different Nt^7 substrates. We challenged this notion and found an interesting selectivity for closely related Nt^7 sequences: mRFP-zDHHC11-KASH induced a strong ONM recruitment of MGSSCSR-Nt^7-GFP but showed a much weaker effect on MGLLCSR-Nt^7-GFP (Supplementary Fig. 6a,b), both sequences commonly found in plant Gα subunits (Supplementary Table 1). Thus, it appears that zDHHC3, 7 and 11 can differentiate among Nt^7 substrates with slight variations in amino acid composition.

We then asked whether the higher PM targeting of Gαo-Nt^{31} compared to Gαo-Nt^7 might also be the outcome of different zDHHC substrate specificities. Thus, we tested if zDHHC3, 7, and 11 target Gαo-Nt^{31} to the ONM with the same efficiency than Gαo-Nt^7. Although the three zDHHC-KASH constructs relocalized Gαo-Nt^{31}-GFP to the ONM, zDHHC3 and zDHHC7 showed a weaker effect when compared to Gαo-Nt^7-GFP (Fig. 6a,b). Therefore, the weaker activity of the Golgi zDHHC3 and 7 toward Gαo-Nt^{31} predicts an increase in its PM accumulation upon time.

Finally, we analyzed if the SpONM system might reveal local S-plamitoylation of the full-length Gαo. Thus, we expressed Gαo-GFP together with the KASH-fusions of zDHHC3, 7, and 11, as they showed activity toward Gαo-Nt^7. Remarkably, full-length Gαo-GFP was targeted to the ONM by all zDHHC constructs (Fig. 6c). On the other hand, the Cys4 mutant of Gαo, MGNC-Gαo-GFP, localized at the ONM primarily when the KASH-fusion for zDHHC11 was co-expressed (Supplementary Fig. 6c), similar to what we observed for MGNC-Nt^7-GFP (Fig. 4d,f,g). Overall, our SpONM system shows that local S-palmitoylation

of Gαo can cause its in-situ accumulation, indicating that zDHHC selectivity and subcellular localization are key players in the substrate compartmentalization.

DISCUSSION

That Gα subunits can be found at the Golgi apparatus is known for almost 30 years[45]. The Golgi localization of Gα subunits was assumed to be part of their trafficking pathway to the cell periphery, although some non-canonical functions of G-proteins were described at compartments other than the PM[46]. Only recently, the Golgi-pool of Gα subunits has been implicated in the downstream signaling of typical GPCRs[4] and the KDEL receptor[5, 6]. Thus, subcellular compartmentalization has emerged as an important player in G protein functions. The present study provides an in-depth characterization of key elements controlling N-myristoylation, S-palmitoylation and localization of Gαo. More importantly, we developed a system – SpONM – for the rapid detection of zDHHC-substrate pair relations in intact cells, opposing the disruptive biochemical and proteomic techniques currently used to study S-palmitoylation[39, 40]. Altogether, this work supports a model in which local S-palmitoylation by distinct zDHHCs is crucial for Gαo compartmentalization, and most likely for other PMPs (Fig. 6d). In this model, N-myristoylation allows the nascent protein to reach virtually the whole endomembrane system. Subsequently, specific PM- and Golgi-localized zDHHCs catalyze S-palmitoylation of PMPs, which in turn accumulate at these compartments. Our model is in agreement with the local S-palmitoylation described for substrates such as PSD95 at dendritic spines[38] and calnexin at the ER[47], but adds the Golgi as a compartment in which PMPs can be locally modified and retained. To our knowledge, S-palmitoylation via the large number of Golgi-localized zDHHCs has been exclusively discussed in the context of Golgi-to-PM transport of integral[48] and PMPs[13]. We hereby challenge the current model and show instead that PMP localization to one compartment or another (including Golgi and PM) is not a consequence of sequential trafficking of the PMPs but rather a direct localization driven by the substrate-specific PAT activities at different compartments.

The fact that zDHHCs can modify multiple substrates has led to the notion that S-palmitoylation is nonspecific and proximity-based. Accordingly, a recent study demonstrated the stochastic S-palmitoylation of engineered Cys in membrane proteins, proposing that catalysis is determined by substrate accessibility and not specific sequence motifs[49]. Several zDHHCs, however, contain PDZ-binding motifs, SH3 domains or ankyrin-repeats outside the catalytic DHHC core that have been implicated in enzyme-substrate interactions[12]. Importantly, our study uncovered a striking substrate specificity for several zDHHCs toward peptides as small as Gαo-Nt[7]. We additionally showed that minor sequence modifications might result not only in drastic changes in the substrate recognition by zDHHCs, but also in the substrate localization (Fig. 6d). Another interesting implication of this model is that cells and tissues could shift the localization – and associated function – of PMPs toward one specific compartment or another by controlling the expression of zDHHCs. The large number

of zDHHC genes and their distinct tissue-specific expression patterns in humans is thus not surprising[35]. This property might be widespread among Metazoa as Nt[7] constructs showed remarkably similar localization in *Drosophila* and mammalian cells, and *Drosophila* contains also a large number of zDHHC genes that are differentially expressed in embryonic and adult tissues[50]. Moreover, it is tempting to speculate that clade-specific zDHHC specializations might account for the distinct Cys position in eukaryotic Gα subunits, especially for Cys at position 5 that dominates in plants and amoebae but is almost absent in Metazoa.

The SpONM system we developed in this study relies on tagging zDHHCs at their C-terminus with the KASH domain of syne-1/nesprin-1 for the ectopic ONM targeting. We applied this strategy only to PM- and Golgi-localized zDHHCs but it might also work for the remaining PATs, excluding zDHHC24 with a predicted C-terminus facing the lumen[40]. Some of the ER-localized zDHHCs, however, showed a prominent ONM localization that might hinder their usage in the SpONM system. In this case, alternative tags for the targeting of ER-localized zDHHCs to the PM, Golgi or mitochondria might be applicable. The C-terminal domain of zDHHCs contains two non-catalytic TTxE and PaCCT (palmitoyltransferase conserved C-terminus) motifs that seem relevant for the overall protein structure[51]. The extreme C-terminal region of zDHHCs appears unstructured and is most likely not involved in the binding and presentation of substrates[12], implying that the fusion of a KASH domain does not interfere with the substrate specificity. Accordingly, our SpONM pointed to zDHHC3, 7, and 11 as the major PATs for Gαo. This result is in agreement with a previous study showing zDHHC3 and 7 as the main PATs for Gαi2, Gαq and Gαs[52], although zDHHC11 activity toward Gα subunits has not been detected. This discrepancy could be explained by a differential turnover rate of PM- and Golgi-localized Gα subunits. For instance, if the turnover of the PM pool of Gαi2 is much faster than its Golgi pool, the S-palmitoylation of Gαi2 by the PM-localized zDHHC11 might have gone unnoticed by the biochemical methods used in that study. The SpONM system might therefore provide an advantage in sensitivity by targeting zDHHCs to the ONM, as even small amounts of a substrate are visible at the ectopic compartment.

A polybasic stretch present in the N-terminal region of all Gα subunits has been implicated in PM binding[53]. The Gαo-Nt[31] construct containing the basic region within the α-helix showed indeed a greater steady-state localization at the PM compared to Gαo-Nt[7]. In the SpONM system, the presence of the α-helix in Gαo-Nt[31] appears to impact substrate recognition by the Golgi-associated zDHHC3 and 7, but not by the PM-localized zDHHC11. Thus, these data point out to a second level of complexity in substrate affinity by zDHHCs, where regions distant from the palmitoylatable Cys might subserve regulatory functions. How the polybasic region in Gαo impacts substrate specificity by zDHHCs remains to be clarified.

S-palmitoylation has gained much attention lately as a potential target for drug discovery to combat pathologies mediated by proteins such as the oncogenic Ras and infectious diseases like malaria caused by *Plasmodium falciparum* or the respiratory syndromes caused by coronaviruses[54-56]. Our SpONM system could enable screens for molecules that perturb site- and zDHHC-specific S-palmitoylation of pathological proteins. This approach may provide an attractive alternative to directly target the desired oncogene (or protein of another pathogenic activity), focusing instead on developing tools to target the zDHHCs controlling the proper (or pathological) localization of the protein. In this regard, zDHHCs can be targeted by the drug discovery efforts. The large number of these enzymes in humans and their distinct expression patterns provide the reasoning to expect the power of such an approach in obtaining the favorable pharmacodynamics with limited side effects. Another approach might aim at targeting the specific zDHHC-substrate interaction pairs; this avenue is expected to deliver even more specific targeted therapies.

To sum up, we have delineated the code describing the Golgi *vs.* PM localization of the G protein Gαo, showed that these two localizations are independent from the traditionally assumed Golgi-to-PM trafficking nor preferential interactions with major lipids, and discovered a universal mechanism controlling PMP localization to its target membrane through substrate selectivity of differently localized PATs. This major insight into the cell biology of protein subcellular localization may pave the way to novel drug discovery principles.

METHODS

Antibodies and reagents

Monoclonal antibodies (mAbs) against flotillin-2 (Cat# 610383) and GM130 (Cat# 610823) were from BD Biosciences, mAb against HA (Cat# 11867423001) from Roche, mAb against mRFP (Cat# sc-101526) from Santa Cruz Biotechnology, mAb against GAPDH (Cat# GTX28245) and polyclonal antibody (pAb) against GFP (Cat# GTX113617) were from GeneTex. Secondary Abs for immunostaining and Western blots were from Jackson ImmunoResearch. DAPI (Cat# 32670) and Cycloheximide (Cat# C4859) were from Sigma-Aldrich, D/D solubilizer (Cat# 635054) from Clontech, VECTASHIELD Mounting Medium (Cat# H-1400) from Vector Laboratories, Glutathione Sepharose beads (Cat# GE17-0756-01) from GE Healthcare, DDD85646 (Cat# 13839) from Cayman Chemical, 2-bromopalmitate (Cat# sc-251714) from Santa Cruz Biotechnology, and Membrane lipid strips (Cat# P-6002) from Echelon Biosciences.

Cell lines and culture conditions

Male mouse neuroblastoma Neuro-2a (N2a; ATCC CCL-131) and female human epithelial HeLa (ATCC CCL-2) cells were maintained in MEM (Thermo Fisher Scientific), supplemented with 10% FCS, 2 mM L-glutamine, 1 mM pyruvate, and 1% penicillin-streptomycin at 37°C and 5% CO_2.

Male *Drosophila* Schneider-2 (S2) cells were maintained in Schneider's Drosophila Medium (Lonza) supplemented with 10% FCS and 1% penicillin-streptomycin at 28°C.

All vector transfections were carried out with X-tremeGENE 9 or HP (Roche) according to manufacturer's instructions.

Plasmids and molecular cloning

The plasmids Gαo-GFP, GalT-GFP, and GalT-mRFP for *Drosophila* expression were previously described[6]. To generate the GFP-fusion of Gαo-Nt^{7} and Gαo-Nt^{31}, the fragments were PCR-amplified (primers listed in Supplementary Table 3) from Gαo-GFP, products were cut with KpnI/AgeI and cloned in frame into the same sites of pEGFP-N1 (Clontech). The Gαo-Nt$^{8-31}$-GFP sequence was PCR-amplified from Gαo-Nt^{31}-GFP, the product cut with KpnI/NotI and used to replace the GFP sequence in pEGFP-N1 cut with the same enzymes. Gαo-Nt^{7}-GFP was used as template for the PCR amplification of the following Nt^{7}-GFP sequences: Gαo-G2L, Gαo-C3N, Gαo-S6A, Gαo-S6C, Gαo-S6G, Gαo-S6T, Gαo-S6F, Gαo-S6N, Gαo-S6R, Gαo-S6V, MGNC, MGNTC, MGCKR, MGCKE, MGCDR, MGCDE, MGCKH, MGCDH, MGSLCSR, MGSSCSR, and MGLLCSR. All PCR products were cut with KpnI/NotI and then used to exchange the corresponding GFP sequence from pEGFP-N1. For

Drosophila expression, the plasmids containing the constructs Gαo-Nt^7-GFP, MGNC-Nt^7-GFP, and MGSLCSR-Nt^7-GFP were cut with EcoRI/NotI and inserts were ligated into the same sites of pAc5.1/V5-HisA (Thermo Fisher Scientific). The full-length Gαo mutants MGNC-Gαo and MGSLCSR-Gαo were PCR-amplified from Gαo-GFP, cut and inserted in frame into the KpnI/ApaI sites of pEGFP-N1. For the generation of Gαo-Nt^7-FM^4-GFP and MGNC-Nt^7-FM^4-GFP, the FM^4 sequence was PCR-amplified from the GFP-FM^4-hGH plasmid (Andrew Peden, University of Sheffield), cut with AgeI/PstI and ligated in frame into the same sites of Gαo-Nt^7-GFP and MGNC-Nt^7-FM^4-GFP. The mRFP-Gβ1 construct was created by exchanging the AgeI/BsrGI mCerulean sequence from mCerulean-Gβ1[57] with the corresponding from pmRFP-C1 (Claudia Stuermer, University of Konstanz). Similarly, the mRFP-Gγ3 was created by substituting the AgeI/BsrGI GFP sequence in the GFP-Gγ3 plasmid[6] with the mRFP sequence. The mRFP-Lact-C2 was done by replacing the AgeI/BsrGI GFP sequence from GFP-Lact-C2 (kindly provided by Gregory Fairn; University of Toronto) with the sequence from pmRFP-C1. MannII-mRFP was created by exchanging the BamHI/NotI sequence from MannII-BFP[58] with the equivalent sequence from pmRFP-N1 (Claudia Stuermer, University of Konstanz). The mRFP-KASH plasmid was cloned by substituting the AgeI/BsrGI GFP sequence in the GFP-KASH plasmid[59] with the analogous sequence from pmRFP-C1. The plasmid for the non-tagged SUN2 expression was cloned by cutting the SUN2-CFP plasmid[60] with EcoRI and BamHI, blunting with Phusion DNA Polymerase (New England Biolabs), and re-ligating the plasmid thus introducing a stop codon in frame with the SUN2 sequence. The mRFP-zDHHC5 construct was cloned by cutting the BamHI/NotI sequence of pCI-neo-Flag-DHHC5[61] and ligating in frame into the BglII/PspOMI sites of pmRFP-C1. For the generation of mRFP-zDHHC5-KASH, the sequence mRFP-zDHHC5 was PCR-amplified from mRFP-zDHHC5, cut with NheI/KpnI and used to exchange the GFP sequence cut with the same enzymes from GFP-KASH. Masaki Fukata (National Institutes of Natural Sciences, Japan) generously provided a collection of 23 mouse zDHHC isoforms cloned into the pEF-Bos-HA plasmid[37]. Slightly different cloning strategies were used for the generation of all mRFP-zDHHC-KASH constructs. Specifically, the zDHHC2, 11 and 18 sequences were PCR-amplified from the corresponding pEF-Bos-HA plasmids, cut with AgeI/KpnI and ligated in frame into the BspEI/KpnI sites of mRFP-KASH. The sequence for zDHHC3, 7, 12, 13, 15, 16, 21, and 25 were PCR-amplified from the original pEF-Bos-HA plasmids, cut with BglII/EcoRI and inserted into the same sites of mRFP-KASH. The zDHHC8 sequence was PCR-amplified from pEF-Bos-HA-DHHC8, cut with XhoI/EcoRI and ligated into the same sites of mRFP-KASH. zDHHC9 was PCR-amplified from pEF-Bos-HA-DHHC9, cut with SacI/BamHI and ligated into the same sites of mRFP-KASH. The zDHHC14 sequence was PCR-amplified from pEF-Bos-HA-DHHC14, cut with AgeI/BamHI and ligated into the BspEI/BamHI sites of mRFP-KASH. The zDHHC17 and

23 were PCR-amplified from the corresponding pEF-Bos-HA plasmids, cut with BglII/HindIII and inserted into the same sites of mRFP-KASH. All inactive DHHS-mutants for the relevant mRFP-zDHHC-KASH and HA-zDHHC constructs were obtained by point mutagenesis. The GFP-fusion of reggie-1/flotillin-2 was previously described[62]. Tamas Balla (National Institutes of Health) kindly provided the FAPP1-PH-GFP plasmid and Bo van Deurs (University of Copenhagen) the GFP-caveolin-1 construct. The GFP-SNAP23[63] and pGEX6P1-GFP-Nanobody[64] plasmids were obtained from Addgene

Structure alignment

The following Gαo structures (PDB IDs) 6g79[17], 6oik[18], and 6k41[19] were aligned using the PyMOL software (pymol.org). The N-terminal α-helix of 6g79 was set as reference to align all structures. A similar alignment was done for the Gαi1 structures 1gg2[20], 5kdo[65], 6ddf[66], 6osa[67], 6n4b[68], 6kpf[69], and 6k42[19], setting the N-terminal α-helix of 5kdo as reference.

Immunofluorescence and microscopy

For microscopy, N2a and HeLa cells were transfected for 7 hr, trypsinized and seeded on poly-L-lysine-coated coverslips in complete MEM for additional 15 hr before fixation. When indicated, cells were seeded in complete MEM supplemented with 10 µM DDD85646 or 100 µM 2-bromopalmitate. S2 cells were transfected for 24 hr, washed one time with PBS, resuspended in complete media, and seeded on poly-L-lysine-coated coverslips for 30 min before fixation. All cells were fixed for 20 min with 4% paraformaldehyde in PBS. For immunostaining, cells were permeabilized for 1 min using ice-cold PBS supplemented with 0.1% Triton X-100, blocked for 30 min with PBS supplemented with 1% BSA, incubated with the primary antibody in blocking buffer for 2 hr at room temperature (RT), washed and subsequently incubated with secondary antibodies and DAPI in blocking buffer for 2 hr at RT. All fluorescent-labelled secondary antibodies were from Jackson ImmunoResearch. Coverslips were finally mounted with Vectashield on microscope slides. Cells were recorded with a Plan-Apochromat 63x/1.4 oil objective on a LSM800 Confocal Microscope and further processed using the ZEN blue software (all Zeiss). When required (see below), mean fluorescence intensity was determined from confocal images using ImageJ (National Institutes of Health).

PM and Golgi accumulation

N2a cells expressing the GFP-fusion constructs were immunostained as indicated above using a mouse monoclonal antibody (mAb) against GM130 to visualize the Golgi apparatus, and a DAPI staining for the nucleus (both not shown in all final images). To avoid interferences due to different expression levels of GFP-constructs among cell population, mean fluorescence intensity was measured at the GM130-positive Golgi region as well as at

the total cell area, and ratio values were used to determine the relative Golgi accumulation of the constructs. Simultaneously, mean fluorescence intensity was determined at an unbroken region of the PM lacking membrane protrusions, and the ratio over total cell fluorescence was used to define relative PM content for each GFP-construct. One-way ANOVA or Student's t-test were used for statistical analysis of ≥50 cells per condition and from at least 3 independent experiments.

Co-localization analysis

N2a cells were transfected and immunostained against GM130 as described above. To determine co-localization of the various GFP constructs and the GM130 signal, an area covering the whole perinuclear region but excluding the PM was selected in confocal images and the Pearson's correlation was calculated using the co-localization tool of ImageJ. The same analysis was done in N2a cells co-expressing the phosphatidylserine biosensor mRFP-Lact-C2[27] and the different GFP-fusions, transfected at equal plasmid ratio. The Golgi marker GalT-GFP was used as control. This analysis was also done in N2a cells co-transfected with GFP-fusions, HA-tagged zDHHCs and MannII-BFP as the Golgi marker (2:4:1 plasmid ratio). One-way ANOVA test was used for statistical analysis of >30 cells per condition.

Co-immunoprecipitation

The recombinant GST-tagged Nanobody against GFP[64] expressed in *Escherichia coli* Rosettagami (Novagen) was purified with glutathione Sepharose 4B beads according to manufacturer's instructions. Protein purity was assessed by SDS-PAGE and Coomassie blue staining.

N2a cells were co-transfected with the different Gαo-GFP constructs and mRFP-Gβ1/Gγ3 at 1:1:1 plasmid ratio. After 24 hr transfection, cells were resuspended with ice-cold GST-lysis buffer (1% Triton X-100 and 10% glycerol in PBS) supplemented with a protease inhibitor cocktail (Roche) and passed 10 times through a 25G needle. Extracts were cleared by centrifugation at 15,000xg for 20 min at 4°C, and supernatants were incubated with 1 µg of purified GST-tagged GFP-Nanobody for 30 min on ice. Then, 20 µL of Glutathione Sepharose 4B beads were added and samples rotated overnight at 4°C. Beads were repeatedly washed with GST-lysis buffer, prepared for SDS-PAGE, and finally analyzed by Western blot using a rabbit polyclonal antibody (pAb) against GFP and a mouse mAb against mRFP. HRP-conjugated secondary pAbs (Jackson ImmunoResearch) were used for enhanced chemiluminescence (ECL) detection. The co-immunoprecipitation was done in duplicate with very similar outcomes.

Crude subcellular fractionation

N2a cells were transfected for 24 hr and cell extracts were prepared using non-denaturing conditions and fractionated by high-speed centrifugation as previously described[62]. Briefly, cells were rinsed twice with PBS and resuspended in hypo-osmotic buffer (20 mM Hepes, pH 7.0) supplemented with a protease inhibitor cocktail. The cell suspension was passed 20 times through a 25G needle, and nuclei and unbroken cells were removed by centrifugation at 700xg for 10 min at 4°C. The supernatant was centrifuged at 100,000xg for 60 min at 4°C. The new supernatant (cytosolic fraction) was directly prepared for SDS-PAGE, and the pellet (membrane fraction) was gently washed with hypo-osmotic buffer and resuspended in GST-lysis buffer supplemented with 0.5% SDS and protease inhibitors. The membrane fraction was cleared by centrifugation at 15,000xg for 20 min at 4°C, and prepared for SDS-PAGE. Western blot analysis was done as above using the pAb against GFP and the mouse mAbs against flotillin-2 and GAPDH as endogenous membrane and cytosolic markers, respectively. Two-way ANOVA was used for statistical analysis of 4-6 independent experiments.

Protein-lipid overlay assay

After 24 hr of transfection, N2a cells were washed twice with TBS (50 mM Tris-HCl, pH 8.0, 150 mM NaCl and 10% glycerol) and cell extracts were prepared as explained above in TBS supplemented with 0.5% Tx-100 and protease inhibitors. Membrane lipid strips were blocked in 3% BSA in TBS supplemented with 0.1% Tween-20 (TBS-T) for 1 hr at 4°C. Then, strips were incubated overnight at 4°C with cleared cell extracts previously diluted 1/10 in TBS-T supplemented with 1% BSA. Strips were incubated first with a pAb against GFP, and then with a secondary HRP-conjugated pAb to detect GFP-constructs bound to lipid dots. The protein-lipid overlay assay was done in duplicate for each condition with very similar results.

Screening of eukaryotic Gα subunits

To identify Gα subunit paralogs in eukaryotic genomes, the full-length amino acid sequence of Gαo was used for search queries in the NCBI protein Blast browser (blast.ncbi.nlm.nih.gov/Blast.cgi). Specifically, species with sequenced genomes were selected from Ensembl databases (ensembl.org) for vertebrates, plants, fungi, metazoa and protist. For the remaining phylogenetic clades, Gα paralogs were found as above and using the NCBI Taxonomy browser (ncbi.nlm.nih.gov/Taxonomy/Browser/wwwtax.cgi) as guide for clade classification. Sequences were manually curated and when annotated as partial were not considered further for this analysis. A total of 262 species were found to express Gα paralogs among the clades Amoebozoa, Discoba, Haptista, Metamonada, Opisthokonta, Sar, and Viridiplantae (Table S1). Logo representation of the unique sequences selected for the different Gαo-Nt[7] categories (Table S2) was done using the WebLogo application[70] and further edited with Inkscape (inkscape.org).

Reverse dimerization assay

HeLa cells were co-transfected with the Golgi marker GalT-mRFP (not shown in all figures) and Gαo-Nt^7-FM^4-GFP, MGNC-Nt^7-FM^4-GFP or GFP-FM^4-hGH (at a 1:3 plasmid ratio), and seeded on poly-L-lysine-coated coverslips for 15 hr as indicated above. Then, cells were incubated for 2 hr at normal culture conditions in MEM supplemented with 20 mM Hepes, pH 7.4 and 50 μM Cycloheximide to block de novo synthesis of proteins. The reverse dimerization was induced by adding fresh MEM supplemented as above plus 1 μM D/D solubilizer for the time indicated in the corresponding figures. For temperature block of Golgi transport, the last two steps were simultaneously performed at 37°C and 20°C. Then, cells were fixed and prepared for microscopy. Quantification of fluorescence intensity at the MannII-mRFP Golgi region was done as described above. Student's t test was used for statistical analysis of ≥40 cells per condition and from 3 independent experiments.

For the live imaging of reverse dimerization, HeLa cells were transfected as above but seeded on μ-Slide-4-wells coverslips (Ibidi). Cell were first incubated for 30 min at 37°C in Hank's Balanced Salt Solution (Gibco) supplemented with 20 mM Hepes, pH 7.4 and 50 μM cyclohexamide. Slides were then mounted on a temperature-controlled stage in a VisiScope CSU-X1 spinning disk confocal system (Visitron Systems) equipped with a Plan-Apochromat 63x/1.4 oil objective on an AxioObserver.Z1 microscope (Zeiss), a Evolve 512 EMCCD Camera (Photometrics), and the VisiView Imaging software (Visitron Systems). Reverse dimerization was induced by adding D/D solubilizer to reach a 1 μM final concentration, and cells were immediately recorded at one image per 5 second for 10 min. For analysis, movies were generated from stacks using ImageJ, and the mean fluorescence intensity of an area at the center of the MannII-mRFP Golgi region was measured from stacks in >10 cells per condition.

S-palmitoylation at the outer nuclear membrane (SpONM)

HeLa cells were co-transfected as above with plasmids encoding the GFP-fusion, SUN2, and control mRFP-KASH or mRFP-zDHHC-KASH at a 1:3:3 plasmid ratio. Cells were then seeded on poly-L-lysine-coated coverslips, fixed and prepared for microscopy. For quantification, mean GFP-fluorescence intensity at the ONM region labelled by the mRFP-KASH fusion was determined using ImageJ. Simultaneously, GFP-fluorescence was measured at a nearby cytosolic region as well, and the ratio ONM over cytosol was used to define the relative ONM content of each GFP-construct. One-way ANOVA or Student's t-test were used for statistical analysis of ≥40 cells per condition and from at least 3 independent experiments.

Statistics and reproducibility

Statistical parameters, including the exact values of n are reported in the figure legends. Results are shown as the mean, and error bars represent the s.e.m. or s.d.; ns, not significant, *$p \leq 0.01$; **$p \leq 0.005$; ***$p \leq 0.001$; ****$p \leq 0.0001$ using one-way or two-way ANOVA with Tukey's post hoc test (for multi-sample groups), and two-sided unpaired Student's *t*-test or Mann-Whitney U test (for two-sample comparison). GraphPad Prism 7 was used to determine statistical significance. No statistical methods were used to predetermine the sample sizes. All replicates successfully reproduced the presented findings.

ACKNOWLEDGEMENTS

The work was supported with the Swiss National Science Foundation grant 31003A_175658 to VLK.

AUTHOR CONTRIBUTIONS

G.P.S. performed and analyzed the experiments, and developed all methodologies. J.V. assisted with protein structural analysis. C.A. assisted with interpretation of results. G.P.S. and V.L.K. designed the work and wrote the paper.

COMPETING INTERESTS

The authors declare no competing interests.

REFERENCES

1. Rosenbaum, D.M., Rasmussen, S.G. & Kobilka, B.K. The structure and function of G-protein-coupled receptors. *Nature* **459**, 356-363 (2009).
2. Hauser, A.S., Attwood, M.M., Rask-Andersen, M., Schioth, H.B. & Gloriam, D.E. Trends in GPCR drug discovery: new agents, targets and indications. *Nat Rev Drug Discov* **16**, 829-842 (2017).
3. Oldham, W.M. & Hamm, H.E. Heterotrimeric G protein activation by G-protein-coupled receptors. *Nat Rev Mol Cell Biol* **9**, 60-71 (2008).
4. Lobingier, B.T. & von Zastrow, M. When trafficking and signaling mix: How subcellular location shapes G protein-coupled receptor activation of heterotrimeric G proteins. *Traffic* **20**, 130-136 (2019).
5. Luini, A. & Parashuraman, S. Signaling at the Golgi: sensing and controlling the membrane fluxes. *Curr Opin Cell Biol* **39**, 37-42 (2016).
6. Solis, G.P. *et al.* Golgi-Resident Galphao Promotes Protrusive Membrane Dynamics. *Cell* **170**, 939-955 e924 (2017).
7. Chen, C.A. & Manning, D.R. Regulation of G proteins by covalent modification. *Oncogene* **20**, 1643-1652 (2001).
8. Farazi, T.A., Waksman, G. & Gordon, J.I. The biology and enzymology of protein N-myristoylation. *J Biol Chem* **276**, 39501-39504 (2001).
9. Linder, M.E. & Deschenes, R.J. New insights into the mechanisms of protein palmitoylation. *Biochemistry* **42**, 4311-4320 (2003).
10. Yuan, M. *et al.* N-myristoylation: from cell biology to translational medicine. *Acta Pharmacol Sin* (2020).
11. Gottlieb, C.D. & Linder, M.E. Structure and function of DHHC protein S-acyltransferases. *Biochem Soc Trans* **45**, 923-928 (2017).
12. Rana, M.S., Lee, C.J. & Banerjee, A. The molecular mechanism of DHHC protein acyltransferases. *Biochem Soc Trans* **47**, 157-167 (2019).
13. Rocks, O. *et al.* The palmitoylation machinery is a spatially organizing system for peripheral membrane proteins. *Cell* **141**, 458-471 (2010).
14. Fukata, M., Sekiya, A., Murakami, T., Yokoi, N. & Fukata, Y. Postsynaptic nanodomains generated by local palmitoylation cycles. *Biochem Soc Trans* **43**, 199-204 (2015).
15. Philippe, J.M. & Jenkins, P.M. Spatial organization of palmitoyl acyl transferases governs substrate localization and function. *Mol Membr Biol* **35**, 60-75 (2019).
16. Castrec, B. *et al.* Structural and genomic decoding of human and plant myristoylomes reveals a definitive recognition pattern. *Nat Chem Biol* **14**, 671-679 (2018).

17. Garcia-Nafria, J., Nehme, R., Edwards, P.C. & Tate, C.G. Cryo-EM structure of the serotonin 5-HT1B receptor coupled to heterotrimeric Go. *Nature* **558**, 620-623 (2018).
18. Maeda, S., Qu, Q., Robertson, M.J., Skiniotis, G. & Kobilka, B.K. Structures of the M1 and M2 muscarinic acetylcholine receptor/G-protein complexes. *Science* **364**, 552-557 (2019).
19. Yuan, D. *et al.* Activation of the alpha2B adrenoceptor by the sedative sympatholytic dexmedetomidine. *Nat Chem Biol* (2020).
20. Wall, M.A. *et al.* The structure of the G protein heterotrimer Gi alpha 1 beta 1 gamma 2. *Cell* **83**, 1047-1058 (1995).
21. Lambright, D.G. *et al.* The 2.0 A crystal structure of a heterotrimeric G protein. *Nature* **379**, 311-319 (1996).
22. Senarath, K. *et al.* Regulation of G Protein betagamma Signaling. *Int Rev Cell Mol Biol* **339**, 133-191 (2018).
23. Xie, Y. *et al.* GPS-Lipid: a robust tool for the prediction of multiple lipid modification sites. *Sci Rep* **6**, 28249 (2016).
24. Kallemeijn, W.W. *et al.* Validation and Invalidation of Chemical Probes for the Human N-myristoyltransferases. *Cell Chem Biol* **26**, 892-900 e894 (2019).
25. Resh, M.D. Trafficking and signaling by fatty-acylated and prenylated proteins. *Nat Chem Biol* **2**, 584-590 (2006).
26. Martinez, A. *et al.* Extent of N-terminal modifications in cytosolic proteins from eukaryotes. *Proteomics* **8**, 2809-2831 (2008).
27. Yeung, T. *et al.* Membrane phosphatidylserine regulates surface charge and protein localization. *Science* **319**, 210-213 (2008).
28. Rivera, V.M. *et al.* Regulation of protein secretion through controlled aggregation in the endoplasmic reticulum. *Science* **287**, 826-830 (2000).
29. Matlin, K.S. & Simons, K. Reduced temperature prevents transfer of a membrane glycoprotein to the cell surface but does not prevent terminal glycosylation. *Cell* **34**, 233-243 (1983).
30. Gordon, D.E., Bond, L.M., Sahlender, D.A. & Peden, A.A. A targeted siRNA screen to identify SNAREs required for constitutive secretion in mammalian cells. *Traffic* **11**, 1191-1204 (2010).
31. Harayama, T. & Riezman, H. Understanding the diversity of membrane lipid composition. *Nat Rev Mol Cell Biol* **19**, 281-296 (2018).
32. Lemonidis, K. *et al.* Substrate selectivity in the zDHHC family of S-acyltransferases. *Biochem Soc Trans* **45**, 751-758 (2017).
33. Dowler, S., Kular, G. & Alessi, D.R. Protein lipid overlay assay. *Sci STKE* **2002**, pl6 (2002).

34. Balla, A., Tuymetova, G., Tsiomenko, A., Varnai, P. & Balla, T. A plasma membrane pool of phosphatidylinositol 4-phosphate is generated by phosphatidylinositol 4-kinase type-III alpha: studies with the PH domains of the oxysterol binding protein and FAPP1. *Mol Biol Cell* **16**, 1282-1295 (2005).
35. Ohno, Y., Kihara, A., Sano, T. & Igarashi, Y. Intracellular localization and tissue-specific distribution of human and yeast DHHC cysteine-rich domain-containing proteins. *Biochim Biophys Acta* **1761**, 474-483 (2006).
36. Ernst, A.M. *et al.* S-Palmitoylation Sorts Membrane Cargo for Anterograde Transport in the Golgi. *Dev Cell* **47**, 479-493 e477 (2018).
37. Fukata, M., Fukata, Y., Adesnik, H., Nicoll, R.A. & Bredt, D.S. Identification of PSD-95 palmitoylating enzymes. *Neuron* **44**, 987-996 (2004).
38. Fukata, Y. *et al.* Local palmitoylation cycles define activity-regulated postsynaptic subdomains. *J Cell Biol* **202**, 145-161 (2013).
39. Peng, T., Thinon, E. & Hang, H.C. Proteomic analysis of fatty-acylated proteins. *Curr Opin Chem Biol* **30**, 77-86 (2016).
40. Zaballa, M.E. & van der Goot, F.G. The molecular era of protein S-acylation: spotlight on structure, mechanisms, and dynamics. *Crit Rev Biochem Mol Biol* **53**, 420-451 (2018).
41. Sosa, B.A., Kutay, U. & Schwartz, T.U. Structural insights into LINC complexes. *Curr Opin Struct Biol* **23**, 285-291 (2013).
42. Lemonidis, K., Sanchez-Perez, M.C. & Chamberlain, L.H. Identification of a Novel Sequence Motif Recognized by the Ankyrin Repeat Domain of zDHHC17/13 S-Acyltransferases. *J Biol Chem* **290**, 21939-21950 (2015).
43. Tonn Eisinger, K.R. *et al.* Palmitoylation of caveolin-1 is regulated by the same DHHC acyltransferases that modify steroid hormone receptors. *J Biol Chem* **293**, 15901-15911 (2018).
44. Li, Y., Martin, B.R., Cravatt, B.F. & Hofmann, S.L. DHHC5 protein palmitoylates flotillin-2 and is rapidly degraded on induction of neuronal differentiation in cultured cells. *J Biol Chem* **287**, 523-530 (2012).
45. Stow, J.L. *et al.* A heterotrimeric G protein, G alpha i-3, on Golgi membranes regulates the secretion of a heparan sulfate proteoglycan in LLC-PK1 epithelial cells. *J Cell Biol* **114**, 1113-1124 (1991).
46. Wedegaertner, P.B. G protein trafficking. *Subcell Biochem* **63**, 193-223 (2012).
47. Lakkaraju, A.K. *et al.* Palmitoylated calnexin is a key component of the ribosome-translocon complex. *EMBO J* **31**, 1823-1835 (2012).
48. Ernst, A.M., Toomre, D. & Bogan, J.S. Acylation - A New Means to Control Traffic Through the Golgi. *Front Cell Dev Biol* **7**, 109 (2019).

49. Rodenburg, R.N.P. *et al.* Stochastic palmitoylation of accessible cysteines in membrane proteins revealed by native mass spectrometry. *Nat Commun* **8**, 1280 (2017).
50. Bannan, B.A. *et al.* The Drosophila protein palmitoylome: characterizing palmitoyl-thioesterases and DHHC palmitoyl-transferases. *Fly (Austin)* **2**, 198-214 (2008).
51. Rana, M.S. *et al.* Fatty acyl recognition and transfer by an integral membrane S-acyltransferase. *Science* **359** (2018).
52. Tsutsumi, R. *et al.* Identification of G protein alpha subunit-palmitoylating enzyme. *Mol Cell Biol* **29**, 435-447 (2009).
53. Kosloff, M., Elia, N. & Selinger, Z. Structural homology discloses a bifunctional structural motif at the N-termini of G alpha proteins. *Biochemistry* **41**, 14518-14523 (2002).
54. Chen, B., Sun, Y., Niu, J., Jarugumilli, G.K. & Wu, X. Protein Lipidation in Cell Signaling and Diseases: Function, Regulation, and Therapeutic Opportunities. *Cell Chem Biol* **25**, 817-831 (2018).
55. Fung, T.S. & Liu, D.X. Post-translational modifications of coronavirus proteins: roles and function. *Future Virol* **13**, 405-430 (2018).
56. Ko, P.J. & Dixon, S.J. Protein palmitoylation and cancer. *EMBO Rep* **19** (2018).
57. Thaler, C., Koushik, S.V., Blank, P.S. & Vogel, S.S. Quantitative multiphoton spectral imaging and its use for measuring resonance energy transfer. *Biophys J* **89**, 2736-2749 (2005).
58. Subach, O.M., Cranfill, P.J., Davidson, M.W. & Verkhusha, V.V. An enhanced monomeric blue fluorescent protein with the high chemical stability of the chromophore. *PLoS One* **6**, e28674 (2011).
59. Espigat-Georger, A., Dyachuk, V., Chemin, C., Emorine, L. & Merdes, A. Nuclear alignment in myotubes requires centrosome proteins recruited by nesprin-1. *J Cell Sci* **129**, 4227-4237 (2016).
60. Turgay, Y. *et al.* SUN proteins facilitate the removal of membranes from chromatin during nuclear envelope breakdown. *J Cell Biol* **204**, 1099-1109 (2014).
61. Tian, H. *et al.* Systematic siRNA Screen Unmasks NSCLC Growth Dependence by Palmitoyltransferase DHHC5. *Mol Cancer Res* **13**, 784-794 (2015).
62. Solis, G.P. *et al.* Reggie/flotillin proteins are organized into stable tetramers in membrane microdomains. *Biochem J* **403**, 313-322 (2007).
63. Kuster, A. *et al.* The Q-soluble N-Ethylmaleimide-sensitive Factor Attachment Protein Receptor (Q-SNARE) SNAP-47 Regulates Trafficking of Selected Vesicle-associated Membrane Proteins (VAMPs). *J Biol Chem* **290**, 28056-28069 (2015).

64. Katoh, Y., Nozaki, S., Hartanto, D., Miyano, R. & Nakayama, K. Architectures of multisubunit complexes revealed by a visible immunoprecipitation assay using fluorescent fusion proteins. *J Cell Sci* **128**, 2351-2362 (2015).
65. Kaya, A.I. *et al.* A Conserved Hydrophobic Core in Galphai1 Regulates G Protein Activation and Release from Activated Receptor. *J Biol Chem* **291**, 19674-19686 (2016).
66. Koehl, A. *et al.* Structure of the micro-opioid receptor-Gi protein complex. *Nature* **558**, 547-552 (2018).
67. Kato, H.E. *et al.* Conformational transitions of a neurotensin receptor 1-Gi1 complex. *Nature* **572**, 80-85 (2019).
68. Krishna Kumar, K. *et al.* Structure of a Signaling Cannabinoid Receptor 1-G Protein Complex. *Cell* **176**, 448-458 e412 (2019).
69. Hua, T. *et al.* Activation and Signaling Mechanism Revealed by Cannabinoid Receptor-Gi Complex Structures. *Cell* **180**, 655-665 e618 (2020).
70. Crooks, G.E., Hon, G., Chandonia, J.M. & Brenner, S.E. WebLogo: a sequence logo generator. *Genome Res* **14**, 1188-1190 (2004).

FIGURE LEGENDS

Figure 1. Key amino acid residues in Gαo N-terminus

a, Amino acid sequence of the GFP-fusion constructs of Gαo N-terminus. **b**-**d**, Representative confocal images of N2a cells expressing full-length Gαo-GFP (top), Gαo-Nt^{7}-GFP (middle) or Gαo-Nt^{31}-GFP (bottom) and immunostained against GM130 as Golgi marker (**b**). Note that while Gαo-Nt^{31}-GFP localizes at the PM and Golgi similar to Gαo-GFP, Gαo-Nt^{7}-GFP targets mainly the Golgi. Color-channels are listed vertically top-to-bottom and selected areas are magnified with the channels displayed also vertically in the same order. DAPI staining in blue marks nuclei. Quantification of mean fluorescence intensity ratios of GFP-fusions at the Golgi (**c**) or PM (**d**) versus total cell. Data shown as the mean ± s.e.m. from 4 independent experiments (Gαo-Nt^{7}, *n*=56; Gαo-Nt^{31}, *n*=61; Gαo, *n*=58). **e**,**f**, Western blot of a crude subcellular fractionation of N2a cells expressing the constructs described in (**b**). Ab against GFP was used for detection of Gαo constructs, and Abs against GAPDH and flotillin-2 (Flot-2) used as cytosolic (Cyto) and membrane (Mem) markers, respectively (**e**). Quantification of the relative distribution of GFP-fusions in cytosolic and membrane fractions (**f**). Data shown as the mean ± s.e.m. from 6 independent experiments. **g**, Images of N2a cells expressing the mutants Gαo-G2L-Nt^{7}-GFP (left) or Gαo-C3N-Nt^{7}-GFP (right) and immunostained against GM130 (not showed in the left panel). Selected region is zoomed-in with DAPI staining in blue. **h**,**i**, Crude fractionation of N2a cells expressing Gαo-Nt^{7}-GFP or the different Nt^{7}-GFP mutants indicated in the figure (**h**). Western blot analysis done as in (**e**). Relative distribution of GFP-fusions in the cytosolic and membrane fractions (**i**). Data shown as the mean ± s.e.m. from 6 independent experiments. **j**, Localization of Gαo-Nt^{7}-GFP in N2a cells under inhibition of N-myristoylation (DDD85646) or S-palmitoylation (2-bromopalmitate; 2-BrPal). **k**,**l**, Localization in N2a cells of mutants of the Serine at position 6 (S6) in Gαo-Nt^{7}-GFP under normal conditions (top) or inhibition of N-myristoylation (bottom). The Ser-to-Cys (S6C) mutant showed a much higher targeting to the PM, quantified in (**l**). Data shown as the mean ± s.e.m. from 4 independent experiments (Gαo-Nt^{7}, *n*=56; S6C, *n*=63). **b**,**g**,**j**,**k**, scale bars, 10 μm. See also Supplementary Fig. 1.

Figure 2. Position of the Cys in Gαo N-terminus

a-**d**, Representative confocal images of N2a cells expressing the Nt^{7}-GFP mutants MGNC (top) or MGNTC (bottom) and immunostained against GM130 (**a**). Note that MGNC-Nt^{7}-GFP localizes strongly at the PM and shows a poor co-localization with the Golgi marker, whereas MGNTC-Nt^{7}-GFP is mostly cytosolic and at the Golgi. Nuclei in blue stained with DAPI. Selected areas are magnified to the right. Quantification of mean fluorescence intensity ratios

of GFP-fusions at the PM versus total cell (**b**). Data shown as the mean ± s.e.m. from 4 independent experiments (Gαo-Nt^7, *n*=56; MGNC-Nt^7, *n*=50; Gαo, *n*=58). Co-localization analysis of the Nt^7-GFP constructs with GM130 (**c**). Data shown as the mean ± s.e.m. from 3 independent experiments (Gαo-Nt^7, *n*=33; MGNC-Nt^7, *n*=36; MGNTC-Nt^7, *n*=39). Localization of MGNC-Nt^7-GFP under inhibition of S-palmitoylation (2-BrPal; **d**). **e**-**g**, Image of N2a cells expressing the MGNC mutant of full-length Gαo (MGNC-Gαo-GFP) and immunostained against GM130 (**e**). DAPI staining in blue. Boxed area is enlarged. Relative localization of GFP-fusions at the PM (**f**). Data shown as the mean ± s.e.m. from 4 independent experiments (Gαo, *n*=56; MGNC-Gαo, *n*=46; MGNC-Nt^7, *n*=50). Co-localization analysis of the constructs with GM130 (**g**). Data shown as the mean ± s.e.m. from 3 independent experiments (Gαo, *n*=47; MGNC-Gαo, *n*=38; MGNTC-Nt^7, *n*=36). **h**-**j**, Logo representations of unique eukaryotic Gα-Nt^7 sequences for the categories Cys3 (**h**), Cys4 (**i**) and Cys5 (**j**). **k**,**l**, N2a cells expressing the Nt^7-GFP construct with the consensus sequence for the Cys5 category (MGSLCSR; **k**). Marked region is magnified. Nucleus stained in blue with DAPI. Full-length Gαo-GFP carrying the Cys5 consensus Nt^7 sequence expressed in N2a cells (**l**). **m**, Localization of Gαo-Nt^7-GFP (top), MGNC-Nt^7-GFP (middle) and MGSLCSR-Nt^7-GFP (bottom) in *Drosophila* S2 cells. Co-expression of GalT-mRFP labels Golgi stacks. Selected areas are zoomed-in to the right. **a**,**e**,**d**,**k**,**l**, scale bars, 10 μm. **m**, scale bars, 5 μm. See also Supplementary Fig. 1 and 2, and Supplementary Tables 1 and 2.

Figure 3. Targeting of Nt^7-GFP

a, Reverse dimerization (RD) assay in HeLa expressing Gαo-Nt^7-FM^4-GFP (left panels) or MGNC-Nt^7-FM^4-GFP (right panels). Cytosolic clusters formed by the Nt^7-FM^4-GFP constructs (top) dissolve by the addition of D/D solubilizer (D/D-Sol, bottom) and show their expected localizations. **b**,**c**, Live imaging of HeLa cells co-expressing Gαo-Nt^7-FM^4-GFP (top) or MGNC-Nt^7-FM^4-GFP (bottom) and the Golgi marker MannII-mRFP (bottom right insets). Representative images of the Nt^7-FM^4-GFP constructs at the time of D/D solubilizer addition (0 min) and after 6 min (**b**). Relative increase upon time of Nt^7-FM^4-GFP constructs at the Golgi region (**c**). Note that Gαo-Nt^7-FM^4-GFP quickly targets the Golgi region, while MGNC-Nt^7-FM^4-GFP only slightly accumulates at the Golgi. Data represent mean ± s.d. (Gαo-Nt^7, *n*=12; MGNC-Nt^7, *n*=11). **d**,**e**, RD assay in HeLa cells expressing MGNC-Nt^7-FM^4-GFP (right) or the secretable control GFP-FM^4-hGH (left) performed at 37°C or at 20°C to inhibit Golgi transport. Incubation with D/D solubilizer results in the almost complete secretion of GFP-FM^4-hGH at 37°C (middle left) but in a Golgi retention at 20°C (bottom left). PM targeting of MGNC-Nt^7-FM^4-GFP seems not affected by the 20°C temperature block (bottom right), and its presence at the Golgi region (MannII-mRFP) is not higher than at 37°C (middle right).

Quantification of mean fluorescence intensity of MGNC-Nt^7-FM^4-GFP, Golgi over total cell (**e**). Data shown as mean ± s.e.m. from 3 independent experiments (37°C, *n*=49; 20°C, *n*=40). **a**,**b**,**d**, scale bars, 10 μm. See also Supplementary Figure 2, and Supplementary Videos 1 and 2.

Figure 4. Local S-palmitoylation at the ONM

a, Schematic representation of core components of the S-palmitoylation at the ONM (SpONM) assay. **b**, Representative images of HeLa cells expressing the constructs mRFP-KASH that targets the ONM, mRFP-zDHHC5 or mRFP-zDHHC5-KASH with or without the co-expression of SUN2 (not shown). Note that mRFP-zDHHC5-KASH efficiently targets the ONM in the presence of SUN2. **c**-**e**, The SpONM assay for Gαo-Nt^7-GFP (**c**) and MGNC-Nt^7-GFP (**d**) using the control mRFP-KASH constructs or mRFP-zDHHC11-KASH. Note that the expression of the KASH-construct carrying zDHHC11 results in the strong recruitment of Gαo-Nt^7-GFP (bottom; **c**) and MGNC-Nt^7-GFP (bottom; **d**) at the ONM, effect not seen by the control mRFP-KASH (top; **c**,**d**). Nuclei stained in blue with DAPI, and marked regions are magnified to the right. Quantification of mean fluorescence intensity ratios of GFP-fusions at the ONM versus cytosol (**e**). Data shown as the mean ± s.e.m. from 3 independent experiments (Gαo-Nt^7 and mRFP-KASH, *n*=44; Gαo-Nt^7 and zDHHC11, *n*=47; MGNTC-Nt^7 and mRFP-KASH, *n*=50; MGNTC-Nt^7 and zDHHC11, *n*=43). **f**-**i**, The SpONM assay using zDHHC3 (**f**) and zDHHC7 (**g**). Gαo-Nt^7-GFP efficiently targets the ONM by the co-expression of mRFP-zDHHC3-KASH (top; **f**) and mRFP-zDHHC7-KASH (top; **g**) in HeLa cells. MGNC-Nt^7-GFP poorly localizes at the ONM in the presence of mRFP-zDHHC3-KASH (bottom; **f**) and mRFP-zDHHC7-KASH (bottom; **g**). DAPI stained nuclei in blue and selected areas are magnified to the right. Quantification of mean fluorescence intensity ratios of GFP-fusions at the ONM versus cytosol by zDHHC3 (**h**) and zDHHC7 (**i**). Data shown as the mean ± s.e.m. from 3 independent experiments (Gαo-Nt^7 and mRFP-KASH, *n*=44; Gαo-Nt^7 and zDHHC3, *n*=50; Gαo-Nt^7 and zDHHC7, *n*=46; MGNTC-Nt^7 and mRFP-KASH, *n*=50; MGNTC-Nt^7 and zDHHC3, *n*=53; MGNTC-Nt^7 and zDHHC7, *n*=45). **b**,**c**,**d**,**f**,**g**, scale bars, 10 μm. See also Supplementary Figures 3 and 4.

Figure 5. zDHHC expression levels drive Nt^7 compartmentalization

a, Gαo-Nt^7-GFP displays its characteristic localization in the SpONM assay using the inactive DHHS mutants for zDHHC3 (zDHHS3, top left), zDHHC7 (zDHHS7, bottom left) and zDHHC11 (zDHHS11, top right) in HeLa cells. The zDHHS11 mutant shows no effect in the localization of MGNC-Nt^7-GFP (bottom right). Boxed areas are zoomed-in to the right, and DAPI labeling nuclei in blue. **b**-**f**, Representative images of N2a cells co-expressing Gαo-Nt^7-

GFP (**b**) or MGNC-Nt^{7}-GFP (**c**,**d**) together with HA-zDHHC11 (top; **b**), HA-zDHHC3 (top; **c**) or HA-zDHHC7 (top; **d**). The corresponding DHHS inactive mutants (bottom; **b**-**d**) were used as controls. Golgi was labelled by the co-expression of MannII-BFP and HA-tagged zDHHCs were immunostained against HA (**b**-**d**). Color-channels are listed vertically top-to-bottom and selected areas are magnified with the channels displayed horizontally in the same order left-to-right. Quantification of mean fluorescence intensity ratios of GFP-fusions at the PM versus total cell (**e**). Data shown as the mean ± s.e.m. from 3 independent experiments (zDHHC11, *n*=61; zDHHS11, *n*=54; zDHHC3, *n*=53; zDHHS3, *n*=56; zDHHC7, *n*=54; zDHHS7, *n*=52). Co-localization analysis of Nt^{7}-GFP constructs with MannII-BFP (**f**). Data represent mean ± s.e.m. from 3 independent experiments (zDHHC11, *n*=53; zDHHS11, *n*=53; zDHHC3, *n*=53; zDHHS3, *n*=51; zDHHC7, *n*=52; zDHHS7, *n*=55). **a**,**b**,**c**,**d**, scale bars, 10 μm. See also Supplementary Figure 5.

Figure 6. Targeting of full-length Gαo to the ONM

a,**b**, The SpONM assay using the control mRFP-KASH, zDHHC3, zDHHC7 and zDHHC11 (**a**). Gαo-Nt^{31}-GFP efficiently targets the ONM by the co-expression of mRFP-zDHHC11-KASH, whereas mRFP-zDHHC3-KASH and mRFP-zDHHC7-KASH induce only a weak ONM recruitment. Quantification of mean fluorescence intensity ratio (ONM versus cytosol) of Gαo-Nt^{31}-GFP compared to Gαo-Nt^{7}-GFP (**b**). Data shown as the mean ± s.e.m. from 3 independent experiments (For Gαo-Nt^{7}: mRFP-KASH, *n*=44; zDHHC3, *n*=50; zDHHC7, *n*=46; zDHHC11, *n*=47. For Gαo-Nt^{31}: mRFP-KASH, *n*=42; zDHHC3, *n*=45; zDHHC7, *n*=41; zDHHC11, *n*=48). **c**, Full-length Gαo-GFP associates with the ONM in the SpONM assay with zDHHC3, zDHHC7 and zDHHC11, but not with the control mRFP-KASH. **d**, Model of how some peripheral membrane proteins might achieve specific subcellular compartmentalization by the interplay of the substrate selectivity of different zDHHCs. The model uses Gαo-Nt^{7}-GFP and MGNC-Nt^{7}-GFP as examples. **a**,**c**, Nuclei stained in blue with DAPI, boxed regions are magnified to the right, and scale bars, 10 μm. See also Supplementary Figure 6.

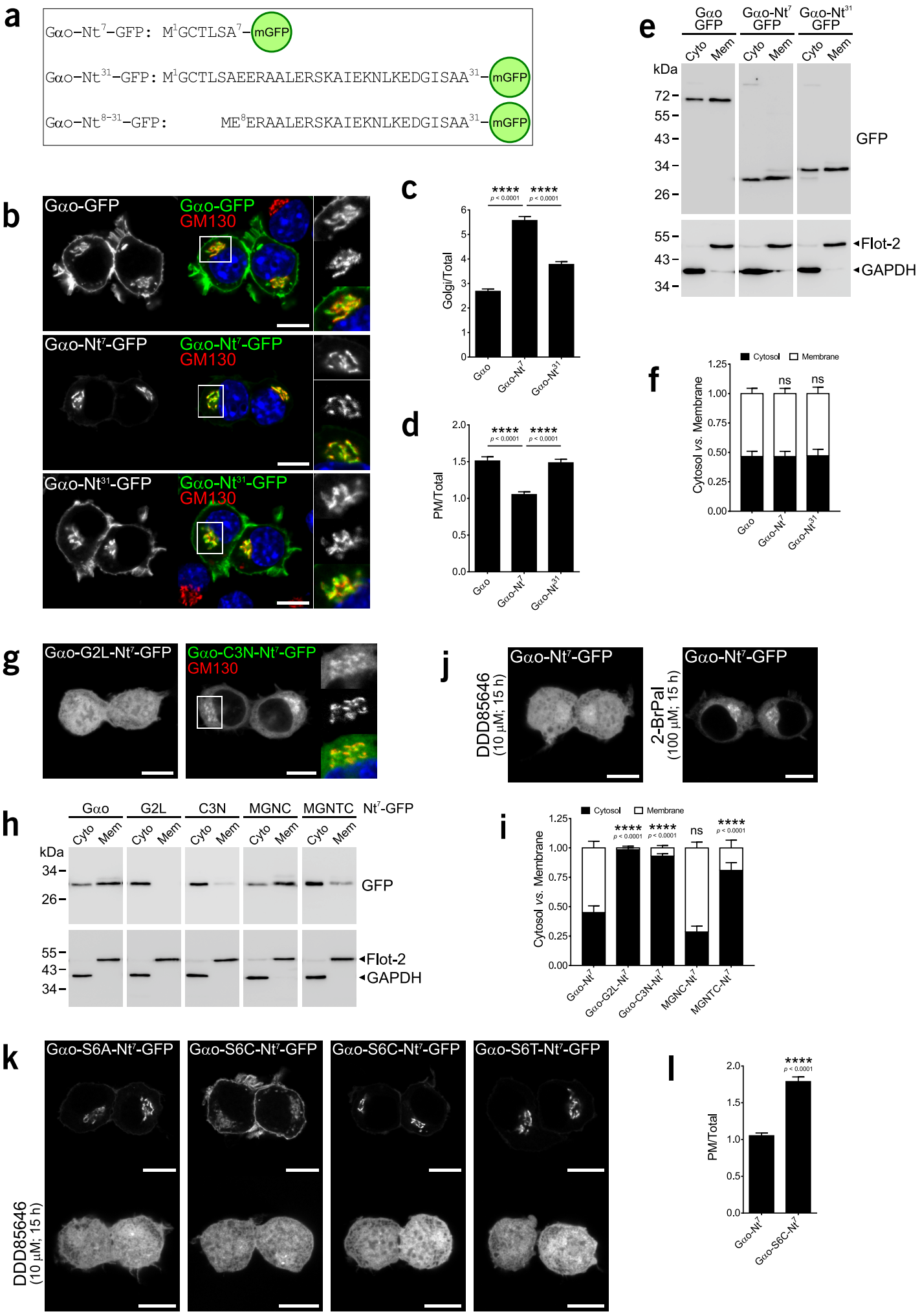

Figure 1_Solis et al.

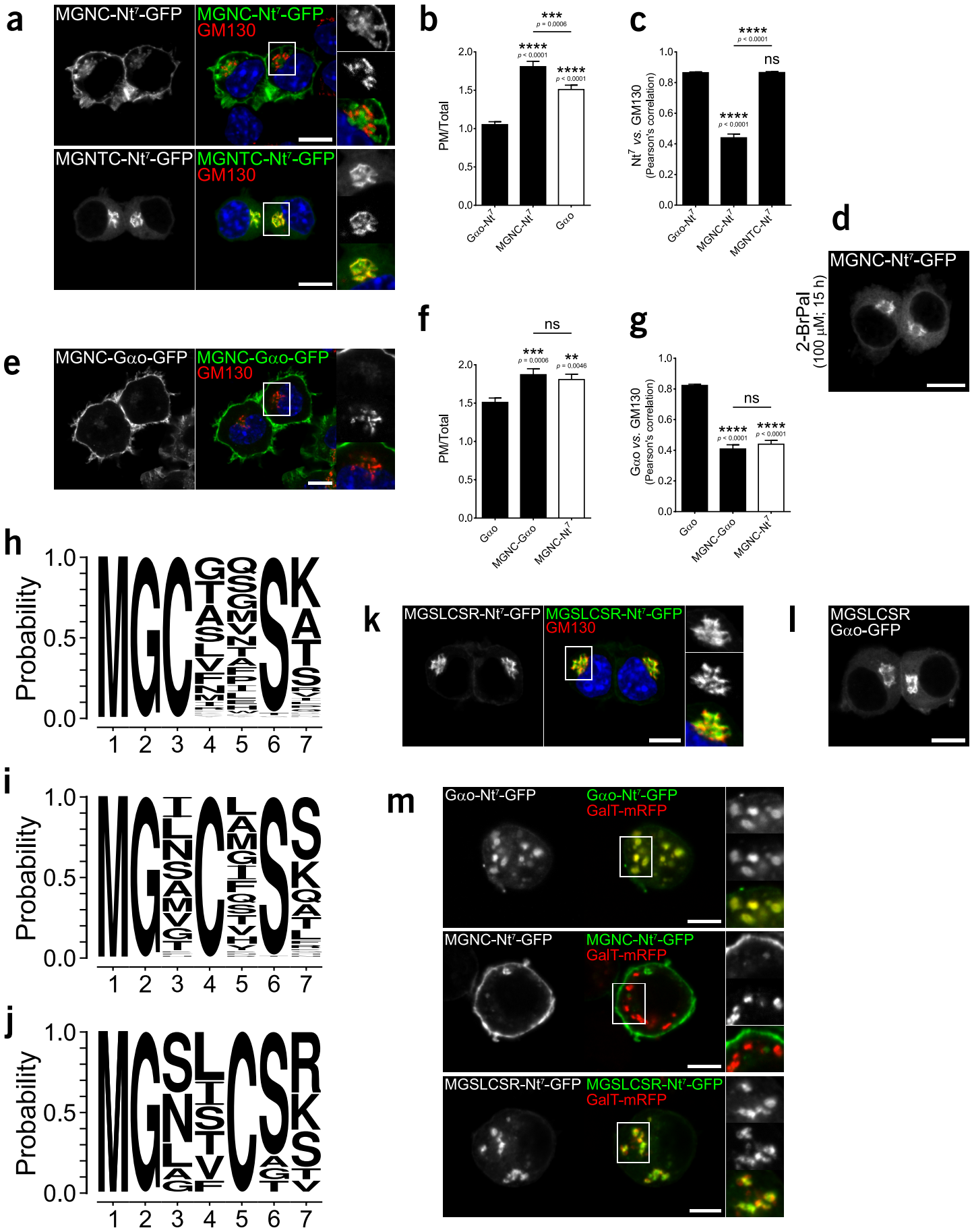

Figure 2_Solis et al.

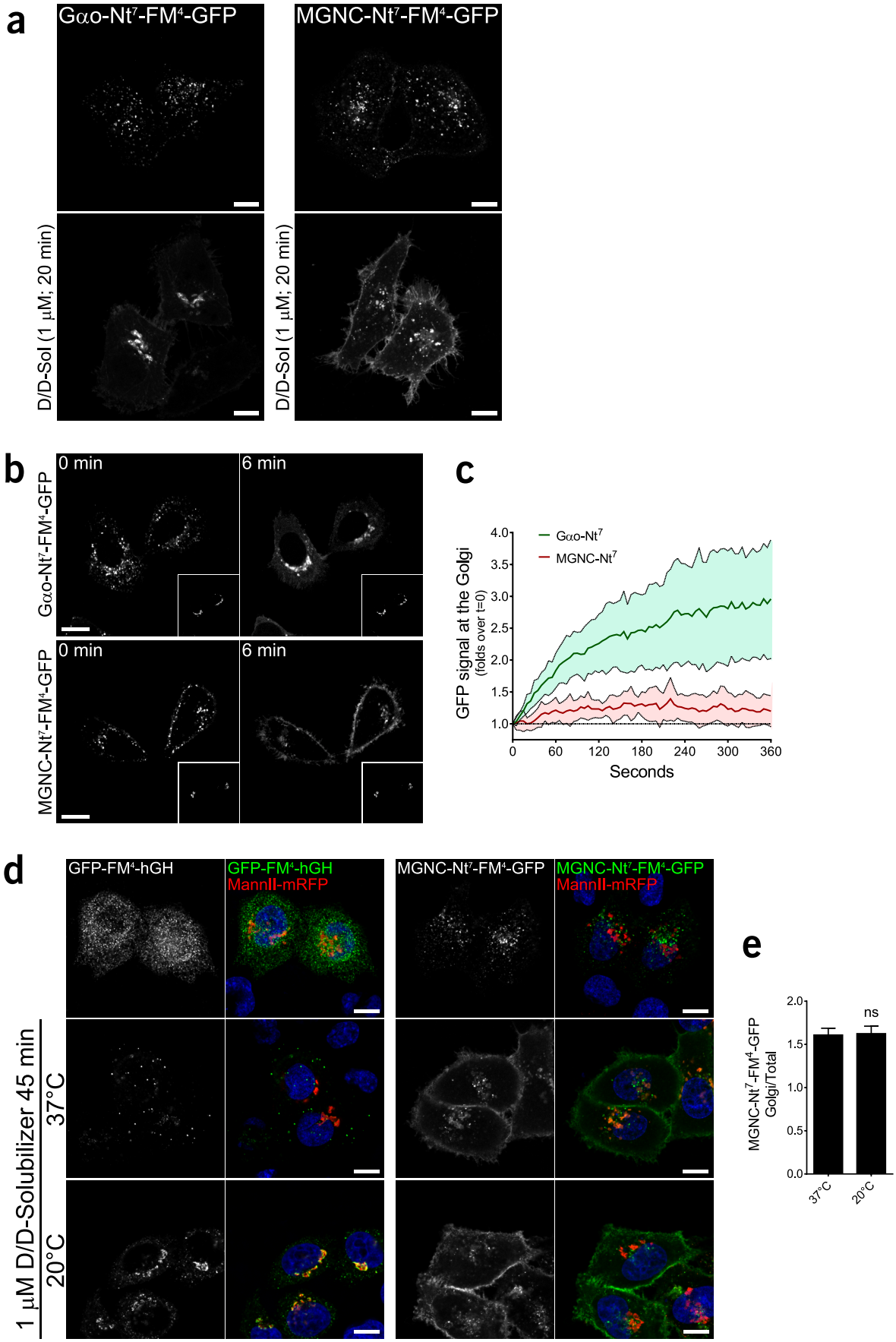

Figure 3_Solis et al.

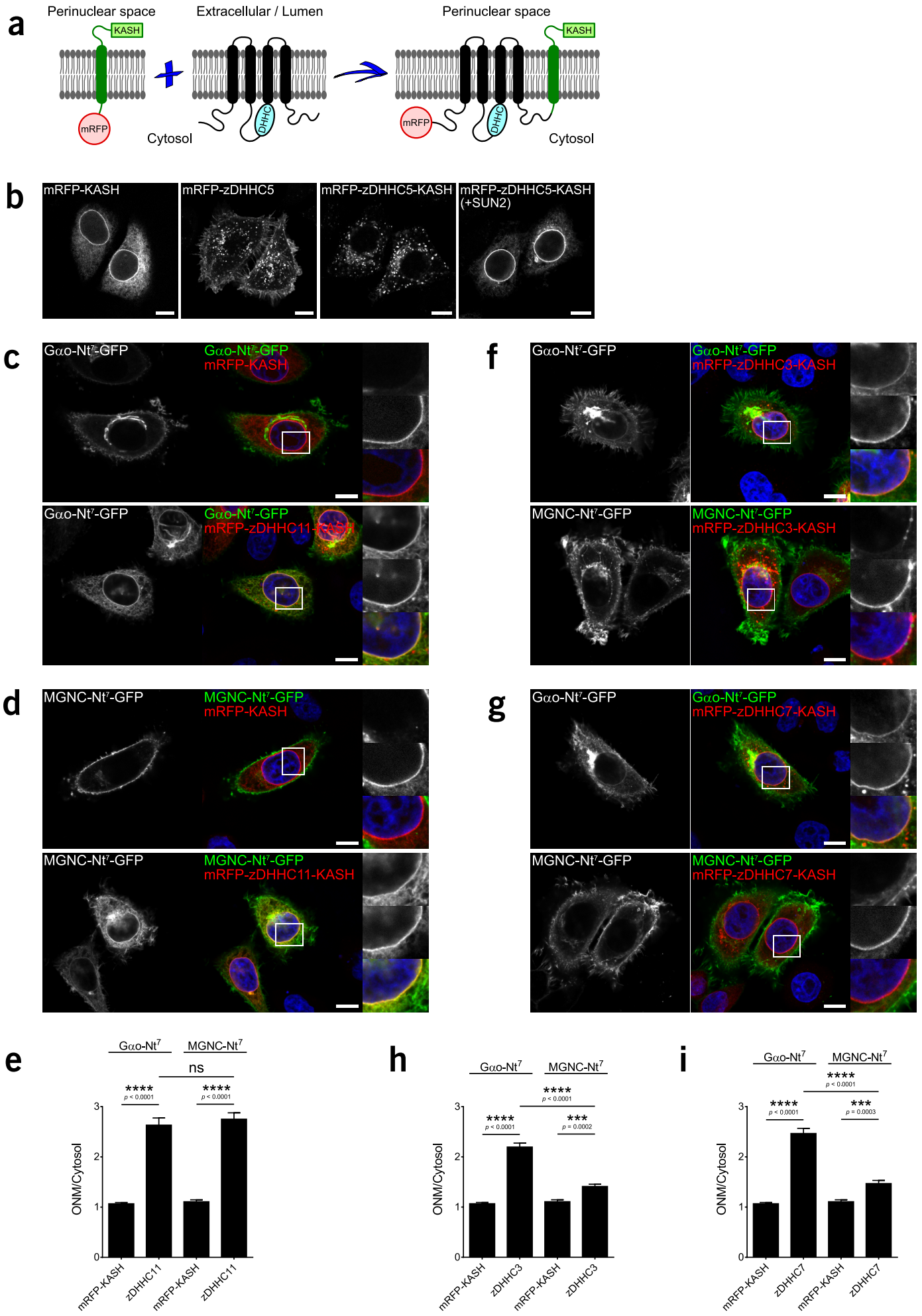

Figure 4_Solis et al.

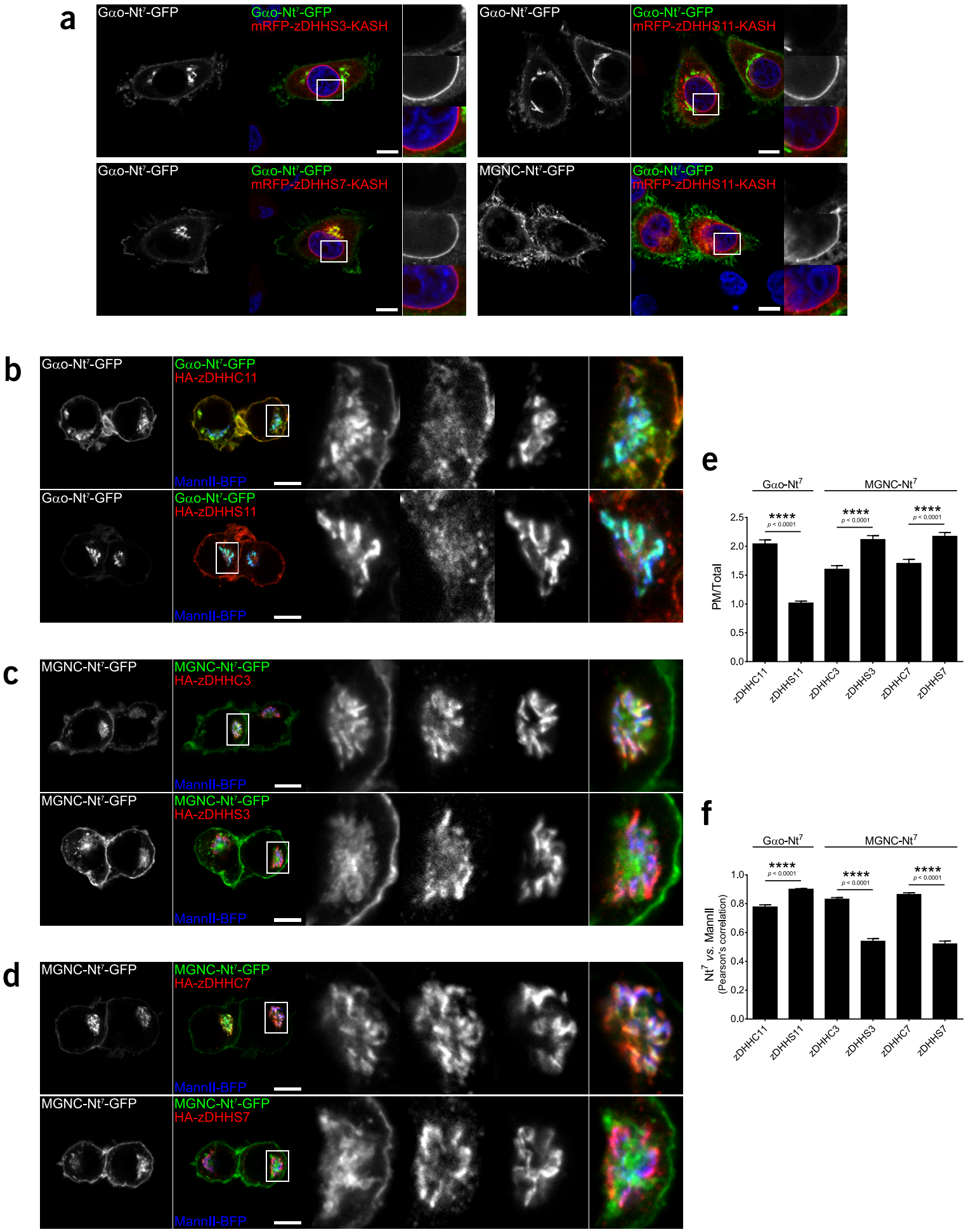

Figure 5_Solis et al.

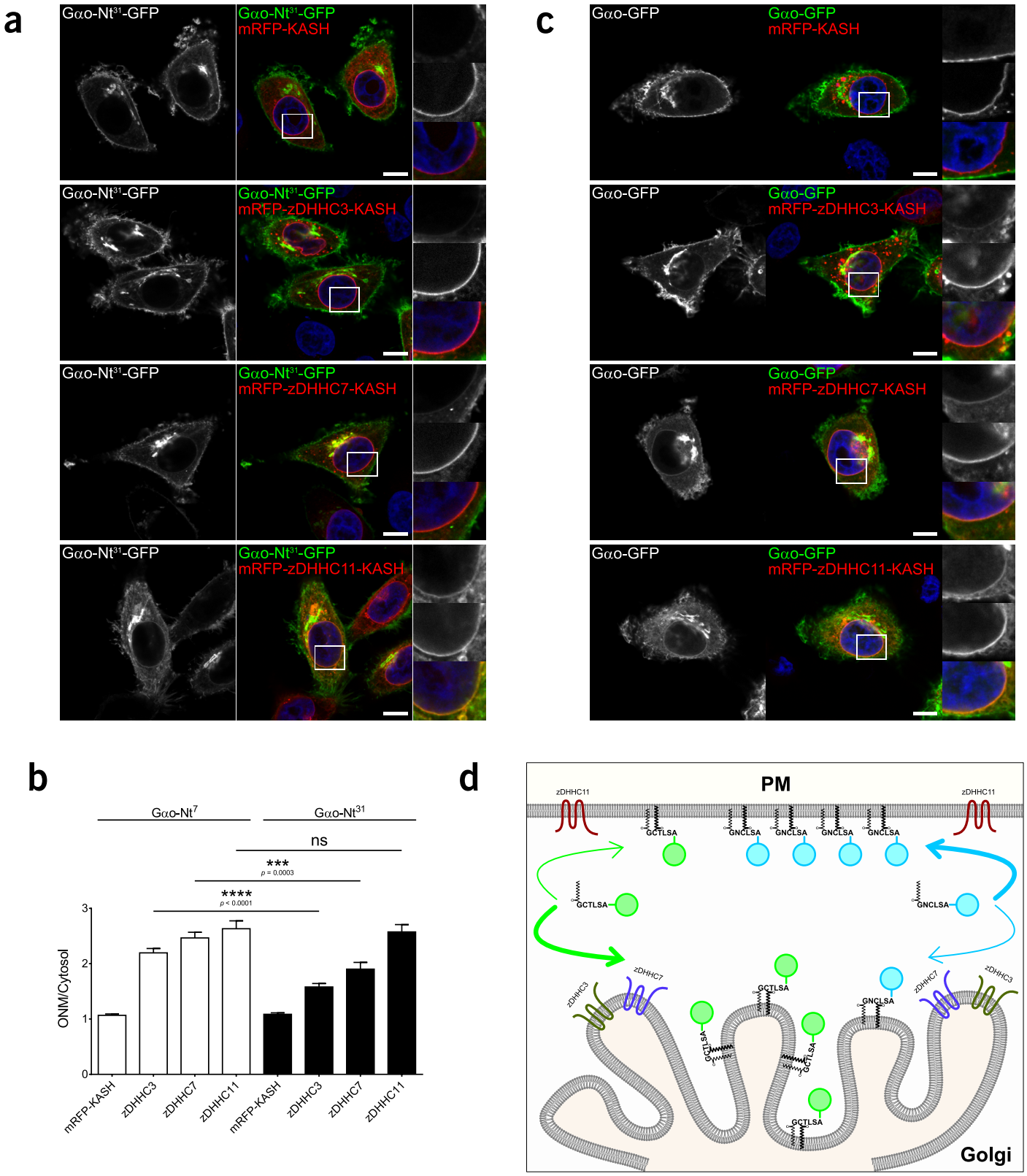

Figure 6_Solis et al.